THE JOURNAL OF BIOLOGICAL CHEMISTRY VOL. 291, NO. 11, pp. 5652–5663, March 11, 2016

Soluble Oligomers of the Pore-forming Toxin Cytolysin A from *Escherichia coli* Are Off-pathway Products of Pore Assembly*

Received for publication, October 27, 2015, and in revised form, January 9, 2016 Published, JBC Papers in Press, January 12, 2016, DOI 10.1074/jbc.M115.700757

Daniel Roderer[‡1], **Stephan Benke**[§], **Benjamin Schuler**[§], **and Rudi Glockshuber**[‡]

From the [‡]*Institute of Molecular Biology and Biophysics ETH Zurich, Otto-Stern-Weg 5, CH-8093 Zurich, Switzerland and the* [§]*Department of Biochemistry, University of Zurich, Winterthurerstrasse 190, CH-8057 Zurich, Switzerland*

The α-pore-forming toxin Cytolysin A (ClyA) is responsible for the hemolytic activity of various *Escherichia coli* and *Salmonella enterica* strains. Soluble ClyA monomers spontaneously assemble into annular dodecameric pore complexes upon contact with membranes or detergent. At ClyA monomer concentrations above ~100 nM, the rate-limiting step in detergent- or membrane- induced pore assembly is the unimolecular reaction from the monomer to the assembly-competent protomer, which then oligomerizes rapidly to active pore complexes. In the absence of detergent, ClyA slowly forms soluble oligomers. Here we show that soluble ClyA oligomers cannot form dodecameric pore complexes after the addition of detergent and are hemolytically inactive. In addition, we demonstrate that the natural cysteine pair Cys-87/Cys-285 of ClyA forms a disulfide bond under oxidizing conditions and that both the oxidized and reduced ClyA monomers assemble to active pores via the same pathway in the presence of detergent, in which an unstructured, monomeric intermediate is transiently populated. The results show that the oxidized ClyA monomer assembles to pore complexes about one order of magnitude faster than the reduced monomer because the unstructured intermediate of oxidized ClyA is less stable and dissolves more rapidly than the reduced intermediate. Moreover, we show that oxidized ClyA forms soluble, inactive oligomers in the absence of detergent much faster than the reduced monomer, providing an explanation for several contradictory reports in which oxidized ClyA had been described as inactive.

Pore-forming toxins (PFTs)[2] exist in different orders of bacteria and eukaryotes and cause various human diseases (1). Some of the most potent bacterial toxins are PFTs, such as anthrax toxin (2) and cytolysin from *Vibrio cholerae* (3). A common feature of all PFTs is the conversion from a soluble, monomeric form into a membrane-embedded oligomeric pore complex (1). The membrane-spanning region of the pore can be formed either by α-helices or β-strands; therefore, PFTs are classified as α-PFTs and β-PFTs (4).

The 34-kDa PFT Cytolysin A (ClyA, also termed Hemolysin E (HlyE)) is an α-PFT existing in various *Escherichia coli* and *Salmonella enterica* strains (5–10). The structure of the annular, dodecameric pore complex of *E. coli* ClyA has been solved to atomic resolution (Protein Data Bank ID: 2WCD) (11). The pore subunit (protomer) shows major structural differences when compared with the soluble ClyA monomer (Protein Data Bank ID: 1QOY) (12): The soluble, monomeric form of ClyA consists of a large tail domain with four long α-helices and one short α-helix (α-helices A, B, C, F, and G; residues 2–159 and 206–303) and a head domain (residues 160–205) with a central, hydrophobic β-hairpin (the "β-tongue," residues 185–195) flanked by two short α-helices (α-helices D and E) (Fig. 1). The tail domain contains a conserved cysteine pair (Cys-87 and Cys-285 in α-helix B and G, respectively) that form a disulfide bond (12–14). During pore formation, ClyA undergoes major structural rearrangements involving more than 50% of all of its amino acids (11). The head domain of the monomer forms elongations of the flanking α-helices (C and F) of the tail domain, and the β-hairpin undergoes a β-to-α transition. The N-terminal α-helix (αA), which is part of the five-helix bundle of the tail domain in the monomer, swings around by 180°, elongating the flanking α-helix B and leaving a four-helix bundle in the protomer (Fig. 1). The remaining four α-helices of the tail domain rearrange to close the gap left by αA (11). The N-terminal half of αA forms the channel through the target cell membrane. The cysteine pair Cys-87/Cys-285 in the reduced protomer remains in spatial proximity with a C_α-C_α distance of 6.8 Å (Fig. 1), which would still enable the formation of a disulfide bond (15). The formation of the assembly-competent protomer is the rate-limiting step (14) and the prerequisite (16) for pore formation.

Recently, a new study on ClyA activation and pore assembly proposed an alternative mechanism of pore assembly (17). The authors discovered two distinct, homo-oligomeric species of ClyA that are formed in the absence of detergent or membranes (termed soluble oligomers below). These oligomers were interpreted as prepores, similar to soluble, oligomeric intermediates in the pore formation of many β-PFTs (18, 19).

* This work was supported by grants from the Swiss National Science Foundation (to R. G. and B. S.) and the National Center of Competence in Structural Biology (to R. G. and B. S.). The authors declare that they have no conflicts of interest with the contents of this article.

[1] To whom correspondence should be addressed: Dept. of Structural Biochemistry, Max Planck Inst. of Molecular Physiology, Otto-Hahn-Strasse 11, D-44227 Dortmund, Germany. Tel.: 49-231-1332312; E-mail: daniel.roderer@mpi-dortmund.mpg.de.

[2] The abbreviations used are: PFT, pore-forming toxin; ClyA, Cytolysin A; $ClyA_{ox}$, oxidized ClyA with Cys-87–Cys-285 disulfide bond; $ClyA_{red}$, reduced ClyA with Cys-87 and Cys-286 in dithiol form; DDM, *n*-dodecyl-β-D-maltopyranoside; FRET, Förster resonance energy transfer; I, intermediate of protomer formation; M, ClyA monomer; Ni^{2+}-NTA, nickel-nitrilotriacetic acid; O, soluble ClyA oligomer: P, ClyA protomer; OMV, outer membrane vesicle; RP-HPLC, reversed phase HPLC; TEV, tobacco etch virus; SO, small oligomer; LO, large oligomer; mOD, milli-optical density unit.

Here we examined this alternative pore formation mechanism of ClyA further. We found no evidence for pore formation or efficient target cell lysis when these soluble oligomers were mixed with detergent or horse erythrocytes, respectively. In fact, the soluble ClyA oligomers showed only 1–2% hemolytic activity relative to ClyA monomers. In addition, no pores could be observed by electron microscopy after incubation of soluble oligomers with detergent (*n*-dodecyl-β-D-maltopyranoside (DDM)) under conditions where the majority of ClyA monomers assembled into dodecameric pore complexes. We therefore interpreted the soluble oligomers as off-pathway products of ClyA pore formation. This conclusion is supported by the finding that the kinetics of soluble oligomer formation coincided with loss in hemolytic activity.

In addition, we compared oligomer formation and hemolytic activity of the reduced, dithiol form of ClyA ($ClyA_{red}$) with pore formation of the oxidized, disulfide form ($ClyA_{ox}$) to address contradictory reports in the literature, which had described $ClyA_{ox}$ either as assembly-incompetent and inactive (13, 17, 20) or as assembly competent (14). In the present study, we show that $ClyA_{ox}$ monomers have essentially the same specific hemolytic activity compared with monomeric $ClyA_{red}$ but form inactive, soluble oligomers 13–14 times faster than $ClyA_{red}$ upon incubation in the absence of detergent or membranes. The results provide a plausible explanation for previous, contradictory reports on the assembly competence of $ClyA_{ox}$.

Finally we also investigated the mechanism of the DDM-induced monomer-to-protomer formation of $ClyA_{ox}$ with single-molecule Förster resonance energy transfer (FRET) measurements, demonstrating that $ClyA_{ox}$ follows the same reaction pathway as $ClyA_{red}$, in which an unstructured off-pathway intermediate (I_{ox}) is formed (21). Due to the lower stability of I_{ox} compared with I_{red}, assembly-competent protomers are even formed one order of magnitude faster from monomeric $ClyA_{ox}$ compared with monomeric $ClyA_{red}$.

Experimental Procedures

Materials—Chemicals of the highest available purity were purchased from Merck KGaA (Darmstadt, Germany) or Sigma-Aldrich. Dithiothreithol (DTT), EDTA and β-mercaptoethanol were obtained from AppliChem. DDM was purchased from Anatrace. Brain total lipid extract was purchased from Avanti Polar Lipids, and horse erythrocytes were obtained from Oxoid AG.

Production and Purification of Reduced ClyA—To exclude any influence of an N- or C-terminal polyhistidine purification tag on the activity and assembly of ClyA, we introduced a TEV (tobacco etch virus) protease cleavage site between the N-terminal His_6 tag and the natural ClyA sequence into the previously described ClyA expression plasmid derived from pET11a (14). ClyA production in *E. coli* was carried out at 20 °C for 15 h, as described (16). ClyA was purified from the soluble fraction of the cell extract by Ni^{2+}-NTA affinity chromatography followed by chromatography on hydroxyapatite as described (14). The N-terminal His_6 tag of ClyA was then cleaved by recombinant His_6-tagged TEV protease (22), and the resulting wild-type ClyA (residues Thr2-Val 303) was obtained in the flow-through of a second Ni^{2+}-NTA affinity chromatography as described (16). All purification steps and the proteolytic cleavage were performed under reducing conditions with buffers containing 2 mM β-mercaptoethanol (when Ni^{2+}-NTA columns were used) or 2 mM DTT. The yield of reduced wild-type ClyA ($ClyA_{red}$) was 16 mg of ClyA/liter of bacterial culture. The concentration of ClyA was determined via its specific absorbance at 280 nm (30370 $M^{-1}cm^{-1}$ for $ClyA_{red}$). The $ClyA_{red}$ monomer was stored in PBS buffer (20 mM potassium phosphate, pH 7.3, 150 mM NaCl, 0.1 mM EDTA) with 2 mM DTT at 4 °C and showed no oligomerization within 7 days.

Preparation and Reduction of Oxidized ClyA—To generate the disulfide-bonded oxidized form of ClyA, $ClyA_{red}$ (40 μM) was incubated in PBS buffer with 0.5 mM $CuCl_2$ (*i.e.* 0.4 mM free $CuCl_2$) as a catalyst of air oxidation for 3–4 h at 22 °C. These conditions guaranteed complete oxidation of the Cys-87/Cys-285 pair of ClyA (see below). Oxidized ClyA ($ClyA_{ox}$) was subsequently dialyzed at 4 °C against PBS containing 2 mM EDTA and subjected to gel filtration on a Superdex 200 column (GE Healthcare Life Sciences) equilibrated with PBS to separate oxidized monomers from oxidized oligomers. The absence of free thiols in the purified oxidized monomers was confirmed by Ellman's assay (23) under denaturing conditions (4.0 M guanidinium chloride, pH 8.0) and by analytical reversed phase HPLC (RP-HPLC) at 30 °C on a Zorbax SB300 C8 column (Agilent) using a water-acetonitrile gradient from 50 to 80% (v/v) acetonitrile in 0.1% trifluoroacetic acid (see Fig. 2*A*). The $ClyA_{ox}$ monomer was stored in PBS buffer without DTT at 4 °C and showed no oligomerization within 1.5 days.

The reduction of $ClyA_{ox}$ (monomer, oligomer, or assembled pore complex in 0.1% DDM) was performed in PBS with 100 mM DTT, pH 7.3, at 37 °C and quantified by RP-HPLC as described previously (16). The reduction of unfolded $ClyA_{ox}$ was carried out in 50 mM MOPS-NaOH, 4.0 M guanidinium chloride, pH 7.3, with 20 mM DTT at 37 °C. Reactions were quenched after different time intervals by the addition of formic acid (12% final concentration), and samples were analyzed via RP-HPLC. The peaks corresponding to oxidized and reduced ClyA were integrated, and the data were evaluated according to pseudo first-order kinetics. The reaction between monomeric $ClyA_{red}$ (4 μM) and oxidized $DsbA_{ox}$ (86 μM, corresponding to the periplasmic DsbA concentration in *E. coli* (24)) at pH 7.3 and 37 °C, was analyzed in the same way.

Purification and Oxidation of Förster Resonance Energy Transfer (FRET) Donor/Acceptor-labeled ClyA for Single-molecule Measurements—A ClyA variant with cysteine residues introduced at positions 56 and 252 (ClyACys) was expressed, purified, and labeled at Cys-56 with Alexa Fluor 488 and at Cys-252 with Alexa Fluor 594 as described previously (21). Air oxidation of the natural cysteine pair Cys-87/Cys-285 in the labeled ClyACys variant (4 μM) was performed by incubation in 50 mM KH_2PO_4/K_2HPO_4 pH 7.4, 150 mM NaCl, 10% (v/v) glycerol, and 0.5 mM $CuCl_2$ for 5 h at 22 °C. Oligomers formed during this reaction were removed from the monomers by gel filtration on a Superdex 75 10/300 column (GE Healthcare Life Sciences) in PBS. The quantitative formation of the disulfide bonded Cys-87–Cys-285 was confirmed by reversed phase HPLC on an XTerra RP8 (30 × 4.6 mm) column (Waters) in

TABLE 1

Single-molecule FRET data sets collected for the kinetic analysis for ClyA protomer and pore formation

Repeats used, number of measurements taken for the specified time; Time window length, size of time windows into which the cumulated measurements were divided; Burst min/max, lower and upper limit of number of photons in a burst to be considered for analysis; NA, not applicable.

Total ClyA concentration	Total measurement time	Repeats used	Time window length	Burst min/max
			s	
100 pM	60 s (microfluidics)	NA	NA	40/300
100 pM	10 min	21	60	80/250
100 pM	30 min	9	180	80/250
100 pM	60 min	2	900	80/250
10 nM	15 min	8	30	80/250
10 nM	60 min	4	300	80/250
100 nM	5 min	24	30	80/250
100 nM	15 min	13	60	80/250
100 nM	30 min	4	300	80/250
100 nM	60 min	2	600	80/250

0.1% (v/v) trifluoroacetic acid using a gradient from 30 to 60% acetonitrile.

Oligomerization of ClyA—Oligomers of reduced or oxidized ClyA were formed in the absence of detergents or lipids by incubation at 37 °C (17). For preparative purposes, $ClyA_{red}$ (40 μM) was incubated overnight at 37 °C in PBS, pH 7.3, and subsequently subjected to gel filtration (Superdex 200) to separate the oligomer from the remaining monomer. In the case of $ClyA_{ox}$, a 4-h incubation at 22 °C (conditions of oxidation of ClyA) resulted in a sufficient amount of oligomeric ClyA (Fig. 2*A*). The kinetics of oligomerization of $ClyA_{ox}$ and $ClyA_{red}$ in PBS at 4 °C or 37 °C were determined by quantification of the respective amount of monomeric or oligomeric ClyA via gel filtration on a ProSEC 300S column (Agilent) after different incubation times, starting with ClyA monomer at 5 μM concentration. The decrease in the monomer over time was fitted mono-exponentially, assuming a unimolecular rate-limiting step, which is consistent with previous findings that oligomer formation is concentration-independent at micromolar monomer concentrations (17).

Negative Stain Transmission Electron Microscopy—To trigger pore formation from monomers, ClyA (2 μM in PBS) was incubated in 0.1% DDM for 1 h at 22 °C. Samples were adsorbed on glow-discharged 300-mesh carbon-coated copper grids (Quantifoil) and negatively stained with 2 mM uranyl acetate. Images were recorded by a KeenView CCD camera using a FEI Morgagni electron microscope operating at an acceleration voltage of 100 kV.

Hemolysis Kinetics—The kinetics of ClyA-dependent lysis of horse erythrocytes were measured as described previously (25) by following the decrease in optical density at 650 nm using a Varian Cary 100 spectrophotometer (Agilent). Horse erythrocytes at a density of 2×10^6 cells/ml in PBS, pH 7.3, were lysed at 37 °C by the addition of ClyA (final monomer concentrations of 2–100 nM). Reactions with $ClyA_{red}$ additionally contained 2 mM DTT. Hemolysis kinetics were evaluated by linearly fitting the data points in the middle of the lysis reaction between 35 and 75% of the initial optical density. The slope of the linear decrease in optical density was defined as the maximum lysis velocity. The linear dependence of the maximum lysis velocity on the concentration of ClyA was defined as the specific hemolytic activity of the different ClyA species (16).

Circular Dichroism (CD) Spectroscopy—The monomer-to-protomer transition and pore assembly of $ClyA_{ox}$ and $ClyA_{red}$ (9 μM) in PBS at 22 °C was initiated by the addition of DDM (final concentration, 0.1% (w/v)) and followed via the CD signal change at 225 nm using a temperature-controlled J715 CD spectrometer (Jasco). Samples of reduced ClyA additionally contained 2 mM DTT. Before and after assembly, the CD spectra of $ClyA_{ox}$ and $ClyA_{red}$ were recorded. The rate-limiting step of the monomer-to-protomer conversion was fitted according to a first-order reaction.

Single-molecule Measurements of $ClyA_{ox}$—Kinetic single-molecule FRET measurements were performed and evaluated essentially as described for the reduced ClyACys variant (21). The measurements were recorded on a modified MicroTime 200 instrument (PicoQuant) using a setup for pulsed interleaved excitation (PIE (26)) with two excitation pulses for the donor dye alternating with a single acceptor pulse. The initial phase of protomer formation was measured in a microfluidic mixer (27), and the later phase as well as the pore formation kinetics was constructed from repeated manual mixing measurements (Table 1). All measurements were done at a nominal concentration of labeled ClyACys of 300 pM in PBS with 0.001% (w/v) Tween 20 and 0.1% (w/v) DDM at 22 °C. For recording pore formation kinetics with FRET, excess unlabeled oxidized WT ClyA was added at 10 or 100 nM to achieve the concentrations required to observe the oligomerization of protomers.

The model fitting of the protomer formation was performed as described for the reduced variant (21). The three populations in the transfer efficiency histograms were fitted with Gaussian distributions, once with free amplitudes and once with the amplitudes determined by the kinetic model. Due to the extensive overlap of the peaks, the position and width of the monomer peak function were fixed to the values from the first histogram measured in the microfluidic chip and to those of a reference measurement for the microfluidic mixing and manual mixing data, respectively. As the intermediate is not sufficiently populated in the manual mixing experiments, the position and width of the peak function of the intermediate were fixed to those of the fit of the microfluidic mixing data. The uncertainties of the fitted rate coefficients were estimated with a bootstrap analysis on the level of the individual photon bursts. New sets of photon bursts were synthesized by random sampling with replacement from the original data. One thousand synthetic data sets were created, and the resulting histogram time series were fitted as described above. The resulting distri-

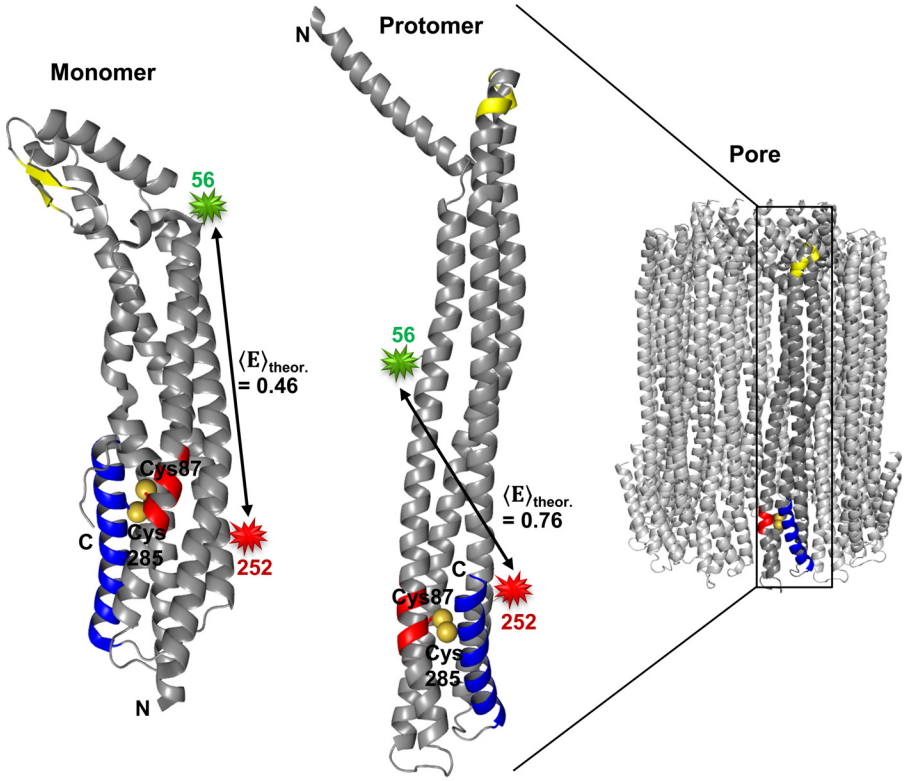

FIGURE 1. **Ribbon diagrams showing the positions of the natural cysteine residues 87 and 285 in the ClyA monomer (*left*) and protomer (*middle*) in the context of the homododecameric ClyA pore (*right*).** The sulfur atoms of both residues are shown as *yellow spheres*. Two additional cysteine residues were introduced for site-specific labeling with Alexa Fluor 488 (*green star*) at position 56 and Alexa Fluor 594 (*red star*) at position 252 for monitoring the monomer-to-protomer transition by FRET. The FRET efficiencies for both conformational states, calculated based on the respective C_α-C_α distances, are indicated. The α-helix G containing Cys-285 is colored *blue*, and segment 81–90 of α-helix B containing Cys-87 is depicted in red. The β-tongue of the ClyA monomer and the respective residues in the ClyA protomer are shown in *yellow*. This figure was prepared using PyMOL (32).

butions of the fit parameters are well described by normal distributions.

Results

Soluble ClyA Oligomers Are Formed Faster by $ClyA_{ox}$ Than by $ClyA_{red}$ and Are Assembly-incompetent—WT ClyA contains a single cysteine pair at positions 87 and 285 that is able to form a disulfide bond in both the monomer and the protomer (14), consistent with the small C_α-C_α distances between the cysteines of 5.2 and 6.8 Å in the structures of the monomer and the protomer, respectively (15) (Fig. 1). Both ClyA redox forms have been described *in vivo*. Although ClyA lacks an N-terminal signal sequence (28), it is secreted to the periplasm where it accumulates in its oxidized form (20, 29). In contrast, the assembled ClyA pore complexes that are exported by the bacteria to the extracellular medium in outer membrane vesicles (OMVs) are composed of reduced ClyA protomers (20). The mechanisms that underlie the secretion of ClyA into the periplasm and its assembly in OMVs are still unknown.

The DDM-induced assembly of ClyA had been characterized in detail for the disulfide-free form of ClyA ($ClyA_{red}$) (21). That study has revealed that the unimolecular formation of assembly-competent protomers (P_{red}) from monomers (M_{red}) is rate-limiting for the formation of dodecameric pore complexes at concentrations above ~100 nM and is accompanied by the reversible formation of a monomeric off-pathway intermediate (I_{red}): $12\ I_{red} \leftrightarrow 12\ M_{red} \leftrightarrow 12\ P_{red} \longrightarrow$ (fast) $\longrightarrow$ dodecameric pore complex.

To study the assembly properties of $ClyA_{ox}$, we first expressed and purified the authentic, untagged ClyA monomer under reducing conditions (2 mM β-mercaptoethanol or DTT) via chromatography of a ClyA variant with an N-terminal His_6 tag on Ni^{2+}NTA-agarose and chromatography on hydroxyapatite followed by specific cleavage of the N-terminal His_6 tag by TEV protease. With this procedure, we obtained pure $ClyA_{red}$ (Thr-2–Val-303), for which Ellman's assay under denaturing conditions confirmed the presence of two thiol groups per polypeptide chain. $ClyA_{ox}$ was obtained from $ClyA_{red}$ after incubation for 4 h with 0.4 mM free $CuCl_2$ as a catalyst of air oxidation in PBS buffer, pH 7.3, at 22 °C in the absence of detergent. Ellman's assay revealed the quantitative formation of the Cys-87–Cys-285 disulfide bond. This was confirmed by a single peak in reversed phase HPLC runs, which allows the quantitative separation of $ClyA_{ox}$ from $ClyA_{red}$ (Fig. 2*B*).

The preparation of $ClyA_{ox}$ was immediately applied to gel filtration, which revealed three distinct species: the oxidized monomer (M_{ox}) and a small (SO_{ox}) and large (LO_{ox}) oligomer of $ClyA_{ox}$ with apparent molecular masses of 580 and 1180 kDa, respectively (Fig. 2*A*). All three $ClyA_{ox}$ species were isolated and again analyzed for quantitative disulfide bond formation by reversed phase HPLC (Fig. 2*B*). The analysis confirmed the presence of the disulfide bond in M_{ox}, SO_{ox}, and LO_{ox} and also showed that purified $ClyA_{red}$ stayed completely reduced, proving to be resistant to air oxidation in the absence of Cu^{2+} (Fig. 2*B*).

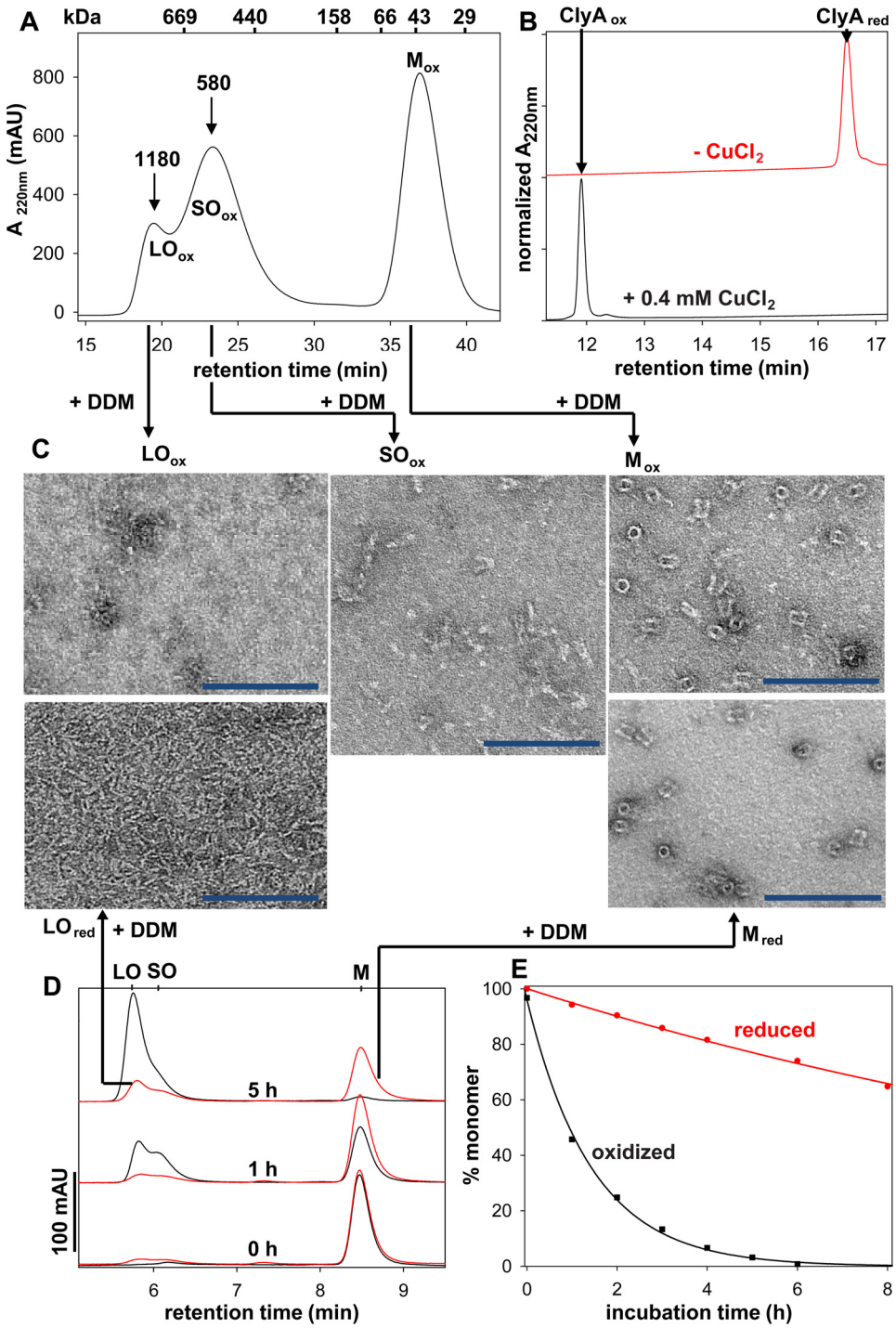

FIGURE 2. **Analysis of spontaneous oligomerization of $ClyA_{ox}$ and $ClyA_{red}$ in the absence of detergent and competence of pore formation of purified ClyA oligomers.** *A*, preparative gel filtration at pH 7.3 of oxidized ClyA after Cu^{2+}-catalyzed air oxidation of $ClyA_{red}$. Besides the oxidized monomer (M_{ox}), a large (LO_{ox}) and a small (SO_{ox}) oligomeric species could be detected. The apparent molecular masses (in kDa) of LO_{ox} and SO_{ox} and the masses of calibration standard proteins are indicated. M_{ox} eluted at an apparent molecular mass of 40 kDa. The height of 100 milliabsorbance units (*mAU*) is indicated. *B*, reversed phase HPLC analysis of ClyA after incubation of $ClyA_{red}$ at pH 7.3 and 22 °C for 3.5 h in the presence or absence of 0.4 mM free $CuCl_2$, showing that $ClyA_{red}$ remained resistant to air oxidation in the absence of $CuCl_2$, whereas it was oxidized quantitatively in the presence of $CuCl_2$. Samples were separated on an analytical C8 column in 0.1% trifluoroacetic acid and eluted with a water/acetonitrile gradient. Due to the denaturing conditions, oligomeric ClyA dissociated so that only a single peak was detected in each run. The HPLC retention times corresponding to $ClyA_{red}$ and $ClyA_{ox}$ are indicated. *C*, negative stain electron micrographs of samples of the purified $ClyA_{ox}$ species LO_{ox}, SO_{ox}, and M_{ox} (see *A*) and the isolated $ClyA_{red}$ species LO_{red} and M_{red} (see *D*) (2 μM total monomer concentration in each sample) after incubation with 0.1% DDM for 1 h at 22 °C. The results show that only M_{ox} and M_{red} were able to form intact pore complexes. *Scale bar*: 100 nm. *D*, comparison of the spontaneous oligomerization propensity of M_{ox} (*black lines*) and M_{red} (*red lines*) (5 μM each) at 37 °C in PBS buffer, pH 7.3. Purified M_{ox} or M_{red} was incubated for 0, 1, or 5 h at 37 °C, and the reaction products were separated at 22 °C in PBS on an Agilent 300S gel filtration column. The results show that M_{ox} has a higher oligomerization tendency than M_{red} and that both redox species can form large and small oligomers. *E*, kinetics of spontaneous oligomerization of M_{ox} and M_{red} (5 μM each) at 37 °C in PBS buffer, pH 7.3, analyzed via the decrease in the monomer peak. Data were normalized to the initial peak area of the monomer and were fitted to a first-order decay (*solid lines*), yielding apparent rate constants of 0.69 ± 0.02 h^{-1} for $ClyA_{ox}$ and 0.052 ± 0.002 h^{-1} for $ClyA_{red}$, respectively.

TABLE 2

Apparent rate constants of the decay of hemolytic activity of M_{red} and M_{ox} as a consequence of spontaneous oligomerization in PBS in the absence of detergent or membranes

ClyA was incubated at 5 μM monomer concentration.

	$ClyA_{red}$	$ClyA_{ox}$
Decrease of hemolytic activities and monomer depletion[a]		
Decrease of hemolytic activity at 37 °C (h^{-1})[b]	$8.5 \pm 0.7 \cdot 10^{-2}$	$5.3 \pm 0.3 \cdot 10^{-1}$
Monomer depletion at 37 °C (h^{-1})[c]	$5.2 \pm 0.2 \cdot 10^{-2}$	$6.9 \pm 0.2 \cdot 10^{-1}$
Decrease in hemolytic activity at 4 °C (h^{-1})[d]	$1.7 \pm 0.1 \cdot 10^{-3}$	$1.1 \pm 0.1 \cdot 10^{-2}$
Monomer depletion at 4 °C (h^{-1})[d]	$4.9 \pm 0.5 \cdot 10^{-4}$	$6.7 \pm 0.2 \cdot 10^{-3}$
Kinetics of I ↔ M ↔ P determined by single-molecule FRET in DDM at 22 °C		
k_{MI} (s^{-1})	$3.0 \pm 0.3 \cdot 10^{-1}$[e]	$1.2 \pm 0.1 \cdot 10^{-1}$[f]
k_{IM} (s^{-1})	$5.0 \pm 1.0 \cdot 10^{-2}$[e]	$1.5 \pm 0.1 \cdot 10^{-1}$[f]
k_{MP} (s^{-1})	$1.7 \pm 0.6 \cdot 10^{-2}$[e]	$4.7 \pm 0.3 \cdot 10^{-2}$[f]
k_{PM} (s^{-1})	$4.7 \pm 0.5 \cdot 10^{-4}$[e]	$8.1 \pm 0.2 \cdot 10^{-3}$[f]

[a] ClyA was incubated at 5 μM monomer concentration.
[b] See Fig. 4*C*.
[c] See Fig. 2*E*.
[d] Data not shown.
[e] Benke *et al.* (21).
[f] Rate constants obtained by single-molecule FRET (see Fig.5*D*).

To test the ability of M_{ox}, SO_{ox}, and LO_{ox} to form dodecameric pore complexes, all species were isolated by gel filtration (Fig. 2*A*) and incubated with 0.1% DDM to trigger pore formation under identical conditions (total monomer concentration of 2 μM, 1-h incubation time, 22 °C, and pH 7.3). Electron microscopy showed that only M_{ox} readily assembled into pores complexes, whereas LO_{ox} and SO_{ox} showed no comparable pore formation activity (Fig. 2*C*, *top panels*).

Next, we found that $ClyA_{red}$ also formed small and large oligomers (SO_{red} and LO_{red}, respectively) in the absence of detergent with the same apparent molecular masses as SO_{ox} and LO_{ox} but with slower assembly kinetics. Fig. 2*D* shows the gel filtration profiles of the kinetics of spontaneous oligomerization of $ClyA_{ox}$ and $ClyA_{red}$ at pH 7.3 and identical initial monomer concentrations of 5 μM, initiated by a temperature shift from 4 to 37 °C. The kinetics of oligomer formation, recorded via the decrease in the peak areas of the monomers, revealed oligomerization half-lives of 60 and 800 min at 37 °C for $ClyA_{ox}$ and $ClyA_{red}$, respectively (Fig. 2*E* and Table 2). Even at 4 °C, slow ClyA oligomerization occurred under these conditions with half-lives of 103 and 1410 h for $ClyA_{ox}$ and $ClyA_{red}$, respectively (Table 2). Together, these results show that the spontaneous formation of the species SO and LO is comparably slow and an intrinsic property of both ClyA redox forms $ClyA_{ox}$ oligomerizes about 14 times faster than $ClyA_{red}$ at both 4 and 37 °C. Oligomerization is strongly favored at the physiological temperature of 37 °C. In addition, Fig. 2*C* demonstrates that M_{ox}, in contrast to previous reports describing the inability of $ClyA_{ox}$ to form pores (20) or its lack of cytotoxicity (13, 17), readily assembles into annular pore complexes.

Fig. 2*D* shows that the small oligomeric form SO_{red} was much less populated than SO_{ox} during spontaneous oligomerization of ClyA in the absence of detergent, so that we could not separate SO_{red} from the much larger LO_{ox} peak. However, we could isolate LO_{red} by preparative gel filtration. Like LO_{ox}, LO_{red} proved to be assembly-incompetent upon the addition of 0.1% DDM, whereas M_{red} efficiently assembled into pore complexes as shown previously (14, 16) (Fig. 2*C*, *lower panels*). Thus, all oligomeric forms of ClyA that formed in the absence of detergent and could be isolated proved to be assembly-incompetent *in vitro* in the presence of DDM in a time frame in which monomeric ClyA was quantitatively incorporated into pores.

The Hemolytic Activity of Oligomeric Forms of Oxidized and Reduced ClyA Is Decreased 100-Fold Relative to the Respective Monomeric Forms—We next tested the ability of the purified oligomeric forms LO_{ox}, SO_{ox}, and LO_{red} to form active pores in target cells. To this end, we compared their lytic activity toward horse erythrocytes with the hemolytic activity of the monomers M_{ox} and M_{red}. Fig. 3*A* shows the hemolysis kinetics at pH 7.3 and 37 °C initiated by mixing erythrocyte suspensions (2×10^6 cells/ml) with LO_{ox}, SO_{ox}, LO_{red}, M_{ox}, or M_{red} at identical total monomer concentrations of 10 nM. The reaction was recorded via the decrease in optical density at 650 nm as a measure of erythrocyte lysis. Whereas M_{ox} and M_{red} proved to be highly active and, after a lag time of about 100 s, caused complete lysis within 200 s, the oligomers LO_{ox}, SO_{ox}, and LO_{red} showed a strongly reduced activity, with lysis half-lives above 2000 s (Fig. 3*A*). For quantification of the specific hemolytic activities of all purified ClyA species, we used the recently established linear dependence of the maximum lysis velocity (see "Experimental Procedures" for the definition) for ClyA concentration in the range of 1 to 100 nM ClyA monomer (16). Fig. 3*B* and Table 3 show that freshly prepared M_{ox} and M_{red} had high specific hemolytic activity, with M_{ox} even 1.2 times more active than M_{red} (1.86 ± 0.14 mOD s^{-1} nM^{-1} and 1.51 ± 0.07 mOD s^{-1} nM^{-1}, respectively). In contrast, the specific activities of the oligomers of $ClyA_{red}$ and $ClyA_{ox}$ were dramatically reduced to 0.9% (LO_{ox} and LO_{red}) and 1.4% (SO_{ox}) of the activity of M_{red} (Fig. 3*B* and Table 3). These results demonstrate that the spontaneous formation of ClyA oligomers in the absence of detergent or membranes inhibits the formation of active pores in target cells. This finding provides strong evidence that the species LO and SO of both ClyA redox forms are off-pathway products of pore formation, reminiscent of oligomeric off-pathway species in the α-PFT equinatoxin II from the sea anemone *Actinia equina* (30) that neither back-react rapidly to active monomers nor integrate into membranes and then become functional pores. The minute hemolytic activity of the oligomers detected in Fig. 3*B* may result from a very slow dissociation of inactive oligomers to active monomers upon dilution to the low ClyA concentration ranges (1–100 nM) used in the hemolysis assays.

The high hemolytic activity of M_{ox} contradicts the previously reported assembly incompetence of oxidized ClyA (13, 17, 20). To test whether the contradictory data in the literature might be the result of the comparably rapid decrease in active monomers in preparations of $ClyA_{ox}$ (Fig. 2*E*), we tested whether the decrease in the concentration of assembly-competent monomers upon oligomerization of $ClyA_{ox}$ and $ClyA_{red}$ coincided with a loss of hemolytic activity. For this purpose, $ClyA_{ox}$ and $ClyA_{red}$ were again incubated under the conditions described in Fig. 2*E*, which favor oligomerization (initial monomer concen-

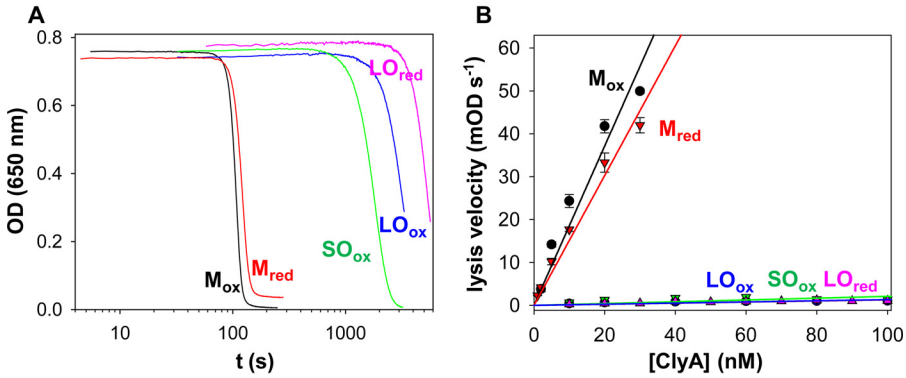

FIGURE 3. **Competence of pore complex formation in the presence of membranes of the different association states of $ClyA_{red}$ and $ClyA_{ox}$.** *A*, hemolytic activity of M, SO, and LO at identical total monomer concentrations of 10 nM. The purified species M_{ox}, SO_{ox}, LO_{ox}, M_{red}, and LO_{red} (10 nM monomer each) were mixed at 37 °C and pH 7.3 with horse erythrocytes (2×10^6 cells/ml). Erythrocyte lysis was followed via the decrease in optical density at 650 nm. Due to its low population, the species SO_{red} could not be purified and separated from LO_{red} by preparative gel filtration. Assays containing reduced ClyA additionally contained 2 mM DTT. *B*, quantification of the specific hemolytic activity of M_{ox}, SO_{ox}, LO_{ox}, M_{red}, and LO_{red} via the linear dependence of maximum lysis velocity on ClyA concentration (see "Experimental Procedures" and Ref. 16 for experimental details), showing that oligomeric species essentially lack hemolytic activity. The maximum lysis velocity (slope of OD_{650} decrease at the half-life of lysis) was plotted against the respective total monomer concentration. The following specific hemolytic activities (in mOD s^{-1} nM^{-1}) were obtained: M_{ox}, 1.86 ± 0.14; M_{red}, 1.51 ± 0.07; LO_{ox}, 0.013 ± 0.002; LO_{red}, 0.013 ± 0.001; SO_{ox}, 0.021 ± 0.005 (indicated errors represent S.D. from three independent measurements).

TABLE 3
Specific hemolytic activities of the different forms of oxidized and reduced ClyA

Sample	Specific hemolytic activity at 37 °C	Specific activity of M_{red}
	mOD s^{-1} nM^{-1}	*%*
M_{ref}	1.51 ± 0.07	100
M_{ox}	1.86 ± 0.14	123
LO_{red}	0.013 ± 0.001	0.9
LO_{ox}	0.013 ± 0.002	0.9
SO_{ox}	0.021 ± 0.005	1.4

tration 5 μM, 37 °C, and pH 7.3). Samples were taken after different time intervals and analyzed for hemolytic activity as described above. Fig. 4 shows the recorded hemolysis profiles and the deduced kinetics of loss of hemolytic activity of $ClyA_{ox}$ and $ClyA_{red}$, which declined within a factor of 1.6 with the same half-lives as the corresponding concentrations of M_{ox} and M_{red} (see Fig. 2*E* and Table 2). At 4 °C, the half-lives of hemolytic activity loss of $ClyA_{ox}$ and $ClyA_{red}$ were about 50-fold longer compared with those recorded at 37 °C (2.6 and 16.9 days, respectively (Table 2)), showing that storage of $ClyA_{ox}$ at 4 °C for 2 weeks leads to practically complete loss of activity. These results thus provide a plausible explanation for the fact that previous experiments had been interpreted such that $ClyA_{ox}$ is assembly-incompetent (13, 17, 20).

$ClyA_{ox}$ Not Only Forms Annular Pore Complexes but Even Assembles Faster Than $ClyA_{red}$—To identify potential differences in the assembly mechanisms of $ClyA_{ox}$ and $ClyA_{red}$, we first compared the kinetics of the monomer-to-protomer transition and the kinetics of pore formation of $ClyA_{ox}$ and $ClyA_{red}$ in the presence of 0.1% DDM by far-UV CD spectroscopy. In the case of $ClyA_{red}$, DDM triggered a rapid CD signal intensity increase, corresponding to the population of the off-pathway intermediate I_{red}, followed by formation of the protomer P_{red} with a more negative CD signal at 225 nm compared with M_{red}, whereas the oligomerization of P_{red} to pore complexes remained spectroscopically silent (14). We observed similar biphasic CD kinetics for $ClyA_{ox}$ at 225 nm (Fig. 5, *A* and *B*). However, the initial increase in the CD signal was less pronounced for $ClyA_{ox}$ (hinting at a lower transient population of the off-pathway intermediate), and the second, rate-limiting step of protomer formation proceeded 7.1 times faster (Fig. 5*B*). The CD spectra and CD kinetics (Fig. 5, *A* and *B*), together with the fact that oxidized and reduced monomers assembled to intact pore complexes in 0.1% DDM (Fig. 2*C*), thus provided a first hint that $ClyA_{ox}$ and $ClyA_{red}$ formed assembly-competent protomers via the same three-state reaction mechanism (I ⇆ M ⇆ P) (21) and that $ClyA_{ox}$ formed protomers faster than $ClyA_{red}$.

To get more quantitative information on the conformational states of $ClyA_{ox}$ populated during DDM-induced protomer formation, we next investigated the kinetics of P_{ox} from M_{ox} by single-molecule FRET experiments as described previously for $ClyA_{red}$ (21). To this end, we used a $ClyA_{ox}$ variant labeled with the FRET pair Alexa Fluor 488 and Alexa Fluor 594 at cysteine residues introduced at position 56 and 252, respectively, showing distinct conformation-specific transfer efficiencies (⟨*E*⟩) for M_{ox}, I_{ox}, and P_{ox} (21) (Fig. 1). We used subnanomolar concentrations of ClyA that prevented protomer assembly, so that only the four unimolecular reactions in the scheme (I_{ox} ⇆ M_{ox} ⇆ P_{ox}) were observed. The time course of the transfer efficiency (⟨*E*⟩) histograms was fully consistent with the expected conversion of M_{ox} (⟨*E*⟩ = 0.42) to P_{ox} (⟨*E*⟩ = 0.67) with the transient population of the off-pathway intermediate I_{ox} (⟨*E*⟩ = 0.20) (Fig. 5*C*). Compared with $ClyA_{red}$ (21) (Fig. 5*D*, *dotted lines*), the formation of P_{ox} was however about one magnitude faster than P_{red} and virtually completed within 200 s (Fig. 5*D*), and the intermediate I_{ox} was less populated. Compared with I_{red}, shown to have molten globule-like characteristics (16, 21), I_{ox} showed an increased transfer efficiency (⟨*E*⟩ = 0.20 *versus* 0.12) (21) (Fig. 5, *C* and *E*), indicating a more compact conformation of I_{ox} in comparison with I_{red}, likely due to the covalent linkage of helices B and G by the Cys-87–Cys-285 disulfide bond. Table 2 compares the microscopic rate constants obtained for the three-state mechanism of protomer formation of $ClyA_{ox}$ and $ClyA_{red}$. The results are that the intermediate I_{ox} is 0.5 kJ/mol less stable than M_{ox}, whereas I_{red} proved to be 4.4 kJ/mol more stable than M_{red} (21). However, P_{ox} was only 4.3 kJ/mol more

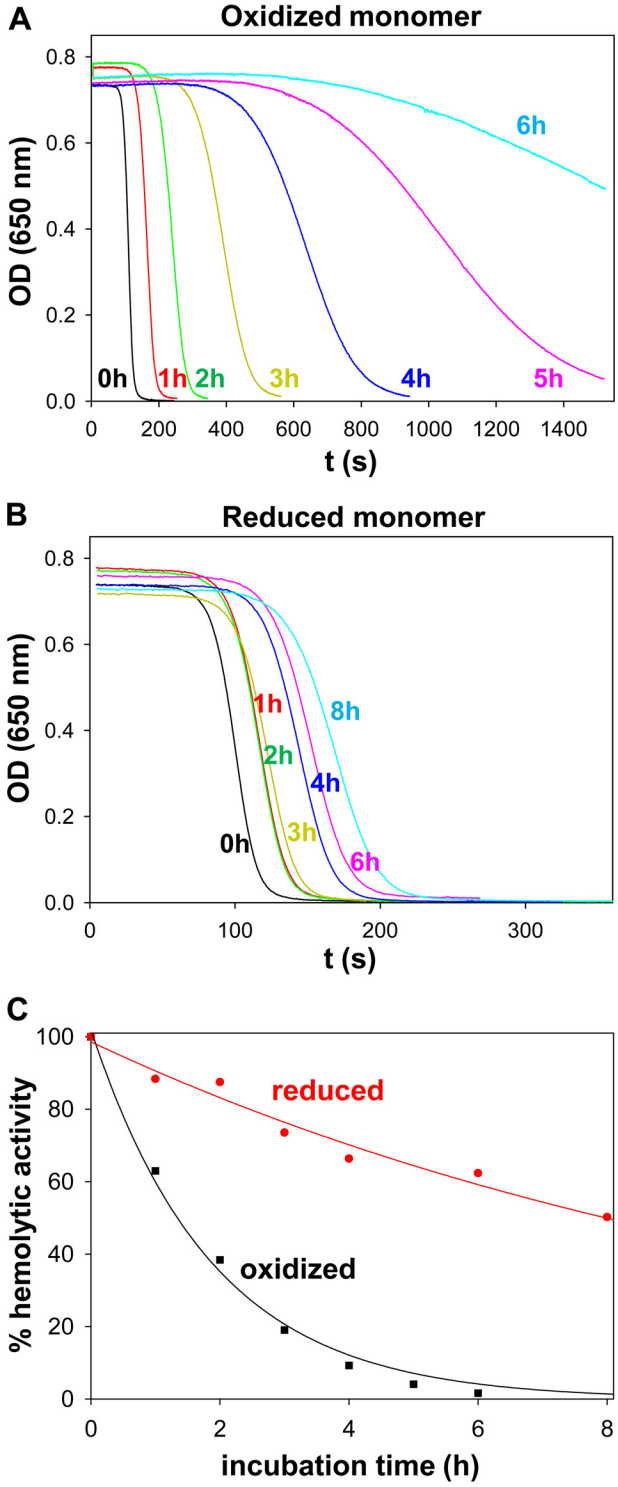

FIGURE 4. **The loss of hemolytic activity of $ClyA_{ox}$ and $ClyA_{red}$ coincides with the decrease in ClyA monomer concentration during spontaneous ClyA oligomerization at 37 °C in the absence of detergent or lipids.** *A* and *B*, hemolysis kinetics initiated by the addition of $ClyA_{ox}$ (*A*) or $ClyA_{red}$ (*B*) after different times of oligomerization to horse erythrocytes. The purified monomers M_{ox} and M_{red} were incubated at 37 °C and pH 7.3 at a concentration of 5 μM for the indicated time intervals an diluted 500-fold with horse erythrocytes (final concentrations, 2×10^6 cells/ml; 10 nM total monomer concentration), and the decrease in cell density was followed via the decrease in the optical density at 650 nm. *C*, kinetics of the decrease in hemolytic activity of $ClyA_{ox}$ and $ClyA_{red}$ at 37 °C and pH 7.3. The maximum lysis velocity as a measure of hemolytic activity (see Fig. 3*B*) was plotted against incubation time. The decay in hemolytic activity yielded apparent rate constants of 0.53 ± 0.03 h^{-1} for $ClyA_{ox}$ and 0.085 ± 0.007 h^{-1} for $ClyA_{red}$, respectively (*solid lines*).

stable than M_{ox}, whereas P_{red} is 8.9 kJ/mol more stable than M_{red} (21) (Fig. 5*F*). Overall, $ClyA_{ox}$ formed the protomer 7–8 times faster than $ClyA_{red}$ upon the addition of DDM (Fig. 5, *B* and *D*), mainly because of a much lower population of the off-pathway intermediate, I (maximum, 30% I_{ox} after 10 s (Fig. 5*D*)) and, to a smaller extent, because of about a two times faster formation of P from M (Table 2).

Finally, we also compared the kinetics of protomer association and pore assembly of $ClyA_{ox}$ and $ClyA_{red}$ by single-molecule FRET experiments at higher protein concentrations (10 nM), which allowed oligomerization to intact pores. This was achieved by adding an excess of the corresponding unlabeled ClyA redox form to donor/acceptor-labeled ClyA as described previously (21) (see also "Experimental Procedures" and the legend to Fig. 5*E* for the details). As observed for $ClyA_{red}$ (21), P_{ox} was converted to a state with lower transfer efficiency ($\langle E \rangle = 0.53$ *versus* 0.67 for P_{ox}) representing a mixture (O_{ox}) of annular pores and emerging, incomplete pores that cannot be distinguished spectroscopically (Fig. 5*E*) (21). These results clearly confirmed the assembly competence of P_{ox} as demonstrated by electron microscopy (see Fig. 2*C*) and hemolysis experiments (Fig. 3). Moreover, the results showed that the assembly of P_{ox} and P_{red} occurred within comparable time frames (Fig. 5*E*). In summary, the single-molecule FRET measurements showed that the DDM-induced monomer-to-protomer transition of $ClyA_{ox}$ follows the same kinetic model as observed for $ClyA_{red}$.

The Disulfide of $ClyA_{ox}$ Is Not Susceptible to Reduction Independently of the Oligomerization State—The *in vivo* role of periplasmic $ClyA_{ox}$ has remained enigmatic, in particular because several groups have reported that $ClyA_{ox}$ has a lower intrinsic hemolytic activity than $ClyA_{red}$ (13, 17, 20), a finding that agrees with the observation that strains deficient in the periplasmic dithiol oxidase DsbA, which introduces disulfide bonds into periplasmic proteins, show ClyA-dependent hemolytic activity, whereas respective wild-type strains are hemolytically inactive (20). To investigate the possibility of a regulated change in the ClyA redox state *in vivo*, we tested the accessibility of the disulfide bond of $ClyA_{ox}$ for reduction by DTT. Fig. 6*A* shows that M_{ox}, LO_{ox}, and oxidized pore complexes were reduced only extremely slowly and remained more than 90% oxidized after 3 h even in 100 mM DTT. In contrast, unfolded M_{ox} was completely reduced within 5 min by 20 mM DTT under the same conditions. The deduced rate constants of reduction (see legend to Fig. 6*A*) revealed that the tertiary structure of M_{ox}, LO_{ox}, and P_{ox} in pore complexes protected the Cys-87–Cys-285 disulfide bond 10^5-10^6-fold against reduction relative to unfolded M_{ox}. The reduction of $ClyA_{ox}$ by disulfide exchange at physiologically relevant rates would thus require unfolding, which is also consistent with the inaccessibility to solvent of the Cys-87/Cys-285 cysteine pair in the structures of the monomer and protomer (Fig. 6*C*). Finally, we also recorded the kinetics of oxidation of M_{red} by DsbA. This reaction also proved to be extremely slow at physiological concentrations of $DsbA_{ox}$ (Fig. 6*B*). The results indicate that the formation of $ClyA_{ox}$ from folded $ClyA_{red}$ in the periplasm via disulfide exchange with DsbA would require the unfolding of M_{red}.

Discussion

The Hemolytic Activity and Pore Formation Competence of $ClyA_{ox}$—In the present study, we addressed two controversies in the literature on the assembly mechanism of ClyA. The first controversy is related to contradictory reports on the ability of $ClyA_{ox}$ to form pore complexes. Several reports have suggested that formation of the Cys-87–Cys-285 disulfide bond in ClyA prevents pore complex formation (13, 17, 20). A loss of assembly competence of $ClyA_{ox}$ was proposed based on the findings that ClyA in OMVs secreted by cytotoxic *E. coli* strains is present in the reduced form and that deletion of the periplasmic dithiol oxidase DsbA, which oxidizes ClyA in the periplasm, restores hemolytic activity (20). In addition, treatment of ClyA with excess Cu(phenanthroline)$_2$, an established reagent for the oxidation of cysteine pairs *in vitro*, led to a loss of hemolytic activity that could be partially recovered by treatment with DTT, and a ClyA variant in which both cysteines were replaced by serine residues stayed active independently of the redox conditions (17). Based on these results, it was speculated that formation of the Cys-87–Cys-285 disulfide bond prevents the conformational transition to the assembly-competent protomers (17). All of these data were however in contrast to previous findings that $ClyA_{ox}$ forms active pores upon the addition of DDM *in vitro* and that both ClyA redox forms show comparable hemolytic activity (14).

We were able to resolve this controversy with our present study, in which we compared the mechanism of DDM-induced assembly of $ClyA_{ox}$ and $ClyA_{red}$ in detail in a quantitative manner. The key proved to be the important recent discovery by Fahie *et al.* (17) that ClyA shows a tendency toward spontane-

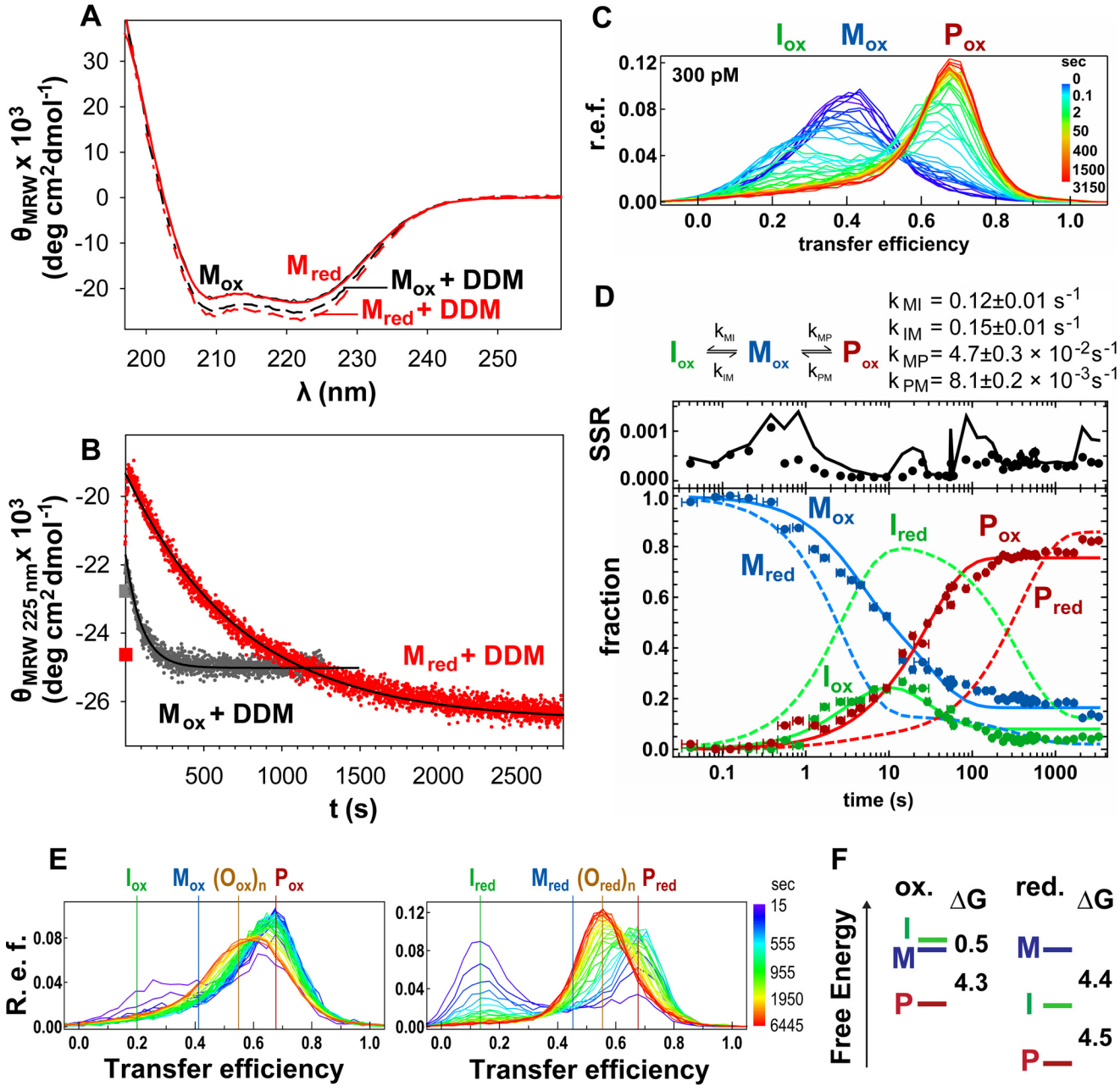

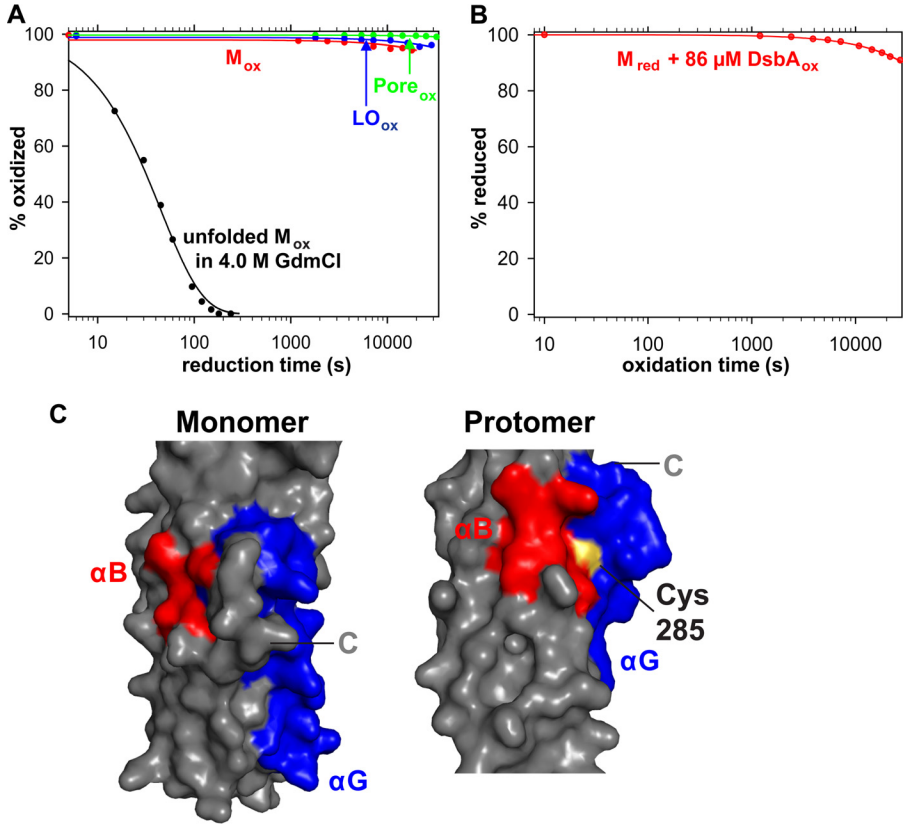

FIGURE 6. **The natural cysteine pair Cys-87/Cys-285 of ClyA is buried and resistant to reduction and oxidation via disulfide exchange.** *A*, kinetics of the reduction of M_{ox}, LO_{ox}, and assembled pores of $ClyA_{ox}$ by 100 mM DTT at 37 °C and pH 7.3, and identical total monomer concentrations of 5 μM (the reaction with assembled pores also contained 0.1% DDM). As a control, unfolded ClyA in 4 M guanidinium chloride was reduced at 37 °C and pH 7.3 with 20 mM DTT. The reactions were stopped after different times by the addition of formic acid (16% final concentration), and oxidized and reduced ClyA was analyzed via RP-HPLC (see Fig. 2*B*). The decrease in the fraction of $ClyA_{ox}$ was fitted according to a pseudo first-order reaction, resulting in rate constants of 1.1 $\pm$ 0.1 M^{-1} s^{-1} for unfolded ClyA, 1.9 $\pm$ 1.1 $\times$ 10^{-5} M^{-1} s^{-1} for M_{ox}, 1.2 $\pm$ 0.2 $\times$ 10^{-5} M^{-1} s^{-1} for LO_{ox}, and 1.9 $\pm$ 0.2 $\times$ 10^{-6} M^{-1} s^{-1} for the oxidized ClyA pore complex. *B*, oxidation of monomeric $ClyA_{red}$ (5 μM) by 86 μM $DsbA_{ox}$ (*in vivo* concentration in *E. coli* (24)) at 37 °C and pH 7.3. The decrease in the fraction of $ClyA_{red}$ was fitted according to a pseudo first-order kinetics, yielding a rate constant of 4.3 $\pm$ 0.1 $\times$ 10^{-2} M^{-1} s^{-1} for the oxidation of $ClyA_{red}$ by $DsbA_{ox}$. *C*, surface representation of the ClyA monomer (*left*) and the ClyA protomer (*right*) in the region around the cysteine pair Cys-87/Cys-285, showing that the sulfur atoms of Cys-87 and Cys-285 are buried in both structures. The positions of α-helixes B (*red*) and G (*blue*) and the C termini are indicated. The sulfur atoms of Cys-87 and Cys-285 are shown as *yellow spheres*. This figure was illustrated in PyMOL (32).

ous formation of larger oligomers in the absence of detergents, in particular at elevated temperatures. We thus compared $ClyA_{ox}$ and $ClyA_{red}$ for their ability to form oligomers spontaneously. For this purpose, we first established the quantitative absence and presence of the Cys-87–Cys-285 disulfide bond in our ClyA preparations (Fig. 2*B*), and we then prepared $ClyA_{ox}$

FIGURE 5. **Both oxidized and reduced ClyA monomers assemble via the same mechanism into functional pore complexes after the addition of the detergent DDM.** *A*, far-UV CD spectra of $ClyA_{red}$ and $ClyA_{ox}$ monomers (*solid lines*) and after assembly to pores in 0.1% DDM at pH 7.3 (*dashed lines*), demonstrating the increased α-helix content of the protomers in the assembled pore complexes. The total monomer concentration in each sample was 9 μM. *B*, reaction of M_{ox} (*gray symbols*) and M_{red} (*red symbols*) to assembly-competent protomers, recorded via the change in the far-UV CD signal at 225 nm. Reactions were initiated by the addition of DDM (manual mixing). The *gray* and *red squares* represent the CD signals of monomeric $ClyA_{ox}$ and $ClyA_{red}$, respectively, in the absence of DDM. The rate-limiting step of monomer-to-protomer transition was fitted monoexponentially, resulting in apparent rates of protomer formation of 9.64 $\pm$ 0.02 $\times$ 10^{-3} s^{-1} and 1.35 $\pm$ 0.01 $\times$ 10^{-3} s^{-1} for $ClyA_{ox}$ and $ClyA_{red}$, respectively. *C* and *D*, single-molecule FRET measurements of the kinetics of the monomer-to-protomer transition of $ClyA_{ox}$ labeled with Alexa Fluor 488 and 594. Protomer formation was initiated by the addition of 0.1% DDM, and the reactions were performed at low ClyA concentrations (300 pM), where oligomerization to pore complexes does not occur (21). CD signal intensities are shown as mean residue molar ellipticity (*MRW*). *C*, transfer efficiency histograms for the monomer-to-protomer transition of $ClyA_{ox}$ in DDM measured by microfluidics and manual mixing. Each *line* represents one histogram normalized to a total area of 1. *Line colors* indicate the reaction time after addition of DDM. The order of the colors is indicated on the *color bar* on the *right*. I_{ox}, off-pathway intermediate; M_{ox}, monomer; P_{ox}, protomer; *r.e.f.*, relative event frequency. *D*, time course of the populations of M_{ox}, I_{ox}, and P_{ox} after initiation of protomer formation by the addition of DDM. *Top panel*, kinetic model with four rate constants used to fit the kinetic data. *Middle panel*, sum of squared residuals (*SSR*) of the kinetic model fit (*line*) and the free population fit (*dots*) to the individual histograms. *Bottom panel*, population time courses for M_{ox}, I_{ox}, and P_{ox} (*blue*, *green*, and *red squares*, respectively) fitted to the model with the off-pathway intermediate indicated at the *top* (*solid lines*). The *dotted lines* indicate the previously determined kinetics of protomer formation of $ClyA_{red}$ under identical conditions and fitted to the same reaction mechanism (21). *E*, dependence on ClyA subunit concentration of the kinetics of DDM-induced pore complex formation of $ClyA_{red}$ and $ClyA_{ox}$ recorded by single-molecule FRET experiments. Conditions were identical to those described in *C* and *D*, but reactions were performed at 10 nM ClyA subunit concentration allowing oligomerization of assembly-competent protomers and pore complex formation. The higher protein concentrations were achieved by mixing 300 pM FRET-labeled ClyA with excess unlabeled WT ClyA with the same redox state. Emerging and final pore complexes of $ClyA_{ox}$ (*left panel*) show identical transfer efficiencies of ~0.53 and appear as a single peak, $(O_{ox})_n$ (*orange*) as observed for $ClyA_{red}$ (*right panel*). The transfer efficiencies of M_{ox}, I_{ox}, and P_{ox} (0.42, 0.20, and 0.67, respectively) and of M_{red}, I_{red}, and P_{red} (21) are also indicated. Transfer efficiency histograms were recorded after different reaction times, with *color codes* indicated in the *bars* at the *top right* of each panel. *F*, schemes of free energies (in kJ/mol) of M, I, and P of $ClyA_{red}$ and $ClyA_{ox}$ in 0.1% DDM at pH 7.3 and 22 °C. The free energies of M_{ox} and M_{red} were assumed to be identical. I_{ox} is 0.5 kJ/mol less stable than M_{ox}, whereas I_{red} is 4.4 kJ/mol more stable than M_{red}. P_{ox} is only 4.3 kJ/mol less stable than M_{ox}, whereas P_{red} is 8.9 kJ/mol more stable than M_{red}.

under mild oxidative conditions by using catalytic concentrations of Cu^{2+} ions for Cu^{2+}-catalyzed air oxidation. We fully confirmed the formation of two main oligomeric species for $ClyA_{red}$ reported previously (17). In addition, however, we showed that $ClyA_{ox}$ forms soluble oligomer 13–14 times faster than $ClyA_{red}$, that oligomer formation is favored at elevated temperatures (Table 2), and that all soluble oligomeric ClyA forms are hemolytically inactive (see below and Table 3). Thus, the formation of assembly-incompetent oligomers in preparations of $ClyA_{ox}$ provides a plausible explanation for the interpretations of previous studies that $ClyA_{ox}$ is hemolytically inactive. Specifically, we have shown that storage of $ClyA_{ox}$ at 4 °C for 3 days already causes a loss of 50% of its hemolytic activity. Therefore, monomers of $ClyA_{ox}$, freshly isolated from gel filtration chromatography, should be used immediately for assembly studies or kept frozen. We also suggest that $ClyA_{red}$ should be prepared and stored in the presence of reducing agents such as DTT to prevent air oxidation.

We analyzed the kinetic mechanism of DDM-induced pore formation for monomeric $ClyA_{ox}$ and $ClyA_{red}$ in detail, which clearly revealed that $ClyA_{ox}$ is not only fully assembly-competent and forms pores with even 20% higher specific hemolytic activity than pores of $ClyA_{red}$ (Fig. 3*B*), but also follows the same reaction mechanism in which the formation of assembly-competent protomers is the rate-limiting step of pore formation at total monomer concentrations above ~100 nM. Protomer formation also is accompanied by the formation of a molten globule-like off-pathway intermediate. Notably, our single-molecule FRET experiments showed that the intermediate I_{ox} is less stable than I_{red} and therefore much less populated during protomer formation, so that assembly-competent protomers P_{ox} even form about one order of magnitude faster than protomers of $ClyA_{red}$ (P_{red}) (Fig. 5). The formation of the Cys-87–Cys-285 disulfide bridge between helixes B and G thus accelerates protomer formation by decreasing the population of off-pathway intermediates during DDM-triggered pore formation.

ClyA in the periplasm of *E. coli* strains containing DsbA has been reported to be oxidized and to exhibit no cytotoxic activity (13, 20). It remains to be established whether $ClyA_{ox}$ also assembles to inactive oligomers in the periplasm, analogous to its spontaneous assembly to oligomers *in vitro*. A recent study reported the co-localization of DsbA and ClyA in OMVs (31), where the reduced form is the main ClyA redox species. Our experiments show that the Cys-87/Cys-285 pair in folded $ClyA_{red}$ monomers cannot be oxidized efficiently by DsbA (Fig. 6*B*). This makes it unlikely that $ClyA_{ox}$ in OMVs needs to be activated by an unknown reducing agent, as proposed previously (20). An alternative explanation for the presence of $ClyA_{red}$ in OMVs could be that $ClyA_{red}$ is the predominant ClyA species in OMVs because it folds rapidly so that DsbA cannot access the Cys-87/Cys-285 pair and the ClyA molecules that stay in the periplasm are oxidized by molecular oxygen under aerobic conditions. Unraveling the translocation mechanism by which ClyA enters the periplasm in a Sec-independent manner appears to be essential for answering this open question.

Are Soluble ClyA Oligomers Really Intermediates of an Alternative Pore Formation Pathway?—Our previous work (21), together with the present data on the kinetic mechanism of DDM-induced pore formation of ClyA, clearly establishes a reaction pathway in which the unimolecular formation of protomers from monomers, with the transient population of a molten globule-like off-pathway intermediate, is the rate-limiting step of pore assembly at ClyA concentrations above ~100 nM. Here, we also examined the alternative ClyA assembly mechanism proposed by Fahie *et al.* (17), in which soluble ClyA oligomers, formed in the absence of detergent or membranes, represent prepores that can integrate into membranes and form hemolytically active pore complexes. We purified soluble oligomers of $ClyA_{ox}$ and $ClyA_{red}$ by gel filtration, but could detect neither a significant population of annular complexes by electron microscopy after addition of detergent (Fig. 2*C*) nor hemolytic activity above 1.4% relative to that of the reduced monomer after mixing the oligomers with erythrocytes (Fig. 3*B*). The interpretation of ClyA oligomers as prepore complexes by Fahie *et al.* (17) is based on findings that the oligomers showed hemolytic activity in end point hemolysis assays (see below) and single-channel conductance activity after reconstitution into planar lipid bilayers. So why did the work of Fahie *et al.* (17) and our present data lead to opposite conclusions on the role of soluble ClyA monomomers?

We believe that the main reason for the interpretation by Fahie *et al.* (17) is the fact that the dependence of hemolytic activity of ClyA oligomers on ClyA concentration was not investigated. Erythrocytes were incubated for 15 min at a total ClyA concentration of 0.8 μM, and the amount of hemoglobin released after 15 min by ClyA oligomers and monomers was compared and used as a measure of hemolytic activity (17). Our Fig. 3, however, shows that the amount of lysed cells at a single time point is not a quantitative measure of hemolytic activity. Instead, the hemolytic activity of ClyA can be quantified accurately only via the dependence of maximum lysis velocity (or the inverse lag time of hemolysis (16)) on ClyA concentration (Fig. 2*B*). Therefore, determination of the specific hemolytic activity of ClyA requires the recording of hemolysis kinetics at different ClyA concentrations. Fig. 3*A* shows that the oligomers LO_{red}, LO_{ox}, and SO_{ox}, already at concentrations of 10 nM, cause significant hemolysis after an incubation time of 1 h, for example, although their specific hemolytic activity relative to the monomer is only about 1%. In fact, ClyA monomers are highly active toxins, and the incubation of erythrocytes with only 10 nM ClyA monomers leads to complete lysis within 200 s (Fig. 3*A*). The experiments by Fahie *et al.* (17) were however performed at 80-fold higher ClyA concentrations, and ClyA activity was deduced from the amount of lysed cells after a single time point (15 min). Fig. 3 shows that we would have detected similarly high hemolytic activity in our preparation of purified ClyA oligomers if we had performed our experiments under the same conditions, *i.e.* at ClyA concentrations of 800 nM.

So what is the reason underlying the low apparent hemolytic activity of ClyA oligomers detected by us and Fahie *et al.*? A rough estimation based on the concentration dependence of ClyA activity (Fig. 3*B*) shows that even a minute fraction of

about 0.1% of monomers spontaneously dissociating from the oligomers and reassembling into active pores via the classical assembly pathway can readily explain the hemolytic and single-channel conductance activity of oligomers detected at the high ClyA oligomer concentrations used by Fahie *et al.* (17). Nevertheless, we cannot completely exclude the possibility that ClyA oligomers react directly to active pores after insertion into erythrocyte membranes, but we believe that this reaction is far too slow to be physiologically relevant.

Author Contributions—R. G., D. R., and B. S. designed the research. S. B. and D. R. prepared protein samples and performed the experiments. D. R., S. B., B. S., and R. G. analyzed and interpreted the data. D. R. and R. G. wrote the manuscript with the help of the other authors.

Acknowledgments—We thank Hiang Dreher and Helene Fäh-Rechsteiner for excellent technical support, Daniel Nettels for discussion and help with data analysis, and Bengt Wunderlich for help in the initial stages of the microfluidic mixing experiments. Electron micrographs were recorded using the equipment of the Scientific Center for Optical and Electron Microscopy (SCOPEM) at ETH Zurich.

References

1. Gonzalez, M. R., Bischofberger, M., Pernot, L., van der Goot, F. G., and Frêche, B. (2008) Bacterial pore-forming toxins: the (w)hole story? *Cell. Mol. Life Sci.* **65,** 493–507
2. Blaustein, R. O., Koehler, T. M., Collier, R. J., and Finkelstein, A. (1989) Anthrax toxin: channel-forming activity of protective antigen in planar phospholipid bilayers. *Proc. Natl. Acad. Sci. U.S.A.* **86,** 2209–2213
3. Olson, R., and Gouaux, E. (2005) Crystal structure of the *Vibrio cholerae* cytolysin (VCC) pro-toxin and its assembly into a heptameric transmembrane pore. *J. Mol. Biol.* **350,** 997–1016
4. Parker, M. W., and Feil, S. C. (2005) Pore-forming protein toxins: from structure to function. *Prog. Biophys. Mol. Biol.* **88,** 91–142
5. del Castillo, F. J., Leal, S. C., Moreno, F., and del Castillo, I. (1997) The *Escherichia coli* K-12 *sheA* gene encodes a 34-kDa secreted haemolysin. *Mol. Microbiol.* **25,** 107–115
6. Ludwig, A., von Rhein, C., Bauer, S., Hüttinger, C., and Goebel, W. (2004) Molecular analysis of cytolysin A (ClyA) in pathogenic *Escherichia coli* strains. *J. Bacteriol.* **186,** 5311–5320
7. Huang, L. J., Cui, J., Piao, H. H., Hong, Y., Choy, H. E., and Ryu, P. Y. (2010) Molecular cloning and characterization of *clyA* genes in various serotypes of *Salmonella enterica*. *J. Microbiol.* **48,** 663–667
8. Oscarsson, J., Westermark, M., Löfdahl, S., Olsen, B., Palmgren, H., Mizunoe, Y., Wai, S. N., and Uhlin, B. E. (2002) Characterization of a pore-forming cytotoxin expressed by *Salmonella enterica* serovars typhi and paratyphi A. *Infect. Immun.* **70,** 5759–5769
9. von Rhein, C., Hunfeld, K. P., and Ludwig, A. (2006) Serologic evidence for effective production of cytolysin A in *Salmonella enterica* serovars typhi and paratyphi A during human infection. *Infect. Immun.* **74,** 6505–6508
10. von Rhein, C., Bauer, S., López Sanjurjo, E. J., Benz, R., Goebel, W., and Ludwig, A. (2009) ClyA cytolysin from *Salmonella*: distribution within the genus, regulation of expression by SlyA, and pore-forming characteristics. *Int. J. Med. Microbiol.* **299,** 21–35
11. Mueller, M., Grauschopf, U., Maier, T., Glockshuber, R., and Ban, N. (2009) The structure of a cytolytic α-helical toxin pore reveals its assembly mechanism. *Nature* **459,** 726–730
12. Wallace, A. J., Stillman, T. J., Atkins, A., Jamieson, S. J., Bullough, P. A., Green, J., and Artymiuk, P. J. (2000) *E. coli* hemolysin E (HlyE, ClyA, SheA): X-ray crystal structure of the toxin and observation of membrane pores by electron microscopy. *Cell* **100,** 265–276
13. Atkins, A., Wyborn, N. R., Wallace, A. J., Stillman, T. J., Black, L. K., Fielding, A. B., Hisakado, M., Artymiuk, P. J., and Green, J. (2000) Structure-function relationships of a novel bacterial toxin, hemolysin E: the role of αG. *J. Biol. Chem.* **275,** 41150–41155
14. Eifler, N., Vetsch, M., Gregorini, M., Ringler, P., Chami, M., Philippsen, A., Fritz, A., Müller, S. A., Glockshuber, R., Engel, A., and Grauschopf, U. (2006) Cytotoxin ClyA from *Escherichia coli* assembles to a 13-meric pore independent of its redox-state. *EMBO J.* **25,** 2652–2661
15. Fass, D. (2012) Disulfide bonding in protein biophysics. *Annu. Rev. Biophys.* **41,** 63–79
16. Roderer, D., Benke, S., Müller, M., Fäh-Rechsteiner, H., Ban, N., Schuler, B., and Glockshuber, R. (2014) Characterization of variants of the pore-forming toxin ClyA from *Escherichia coli* controlled by a redox switch. *Biochemistry* **53,** 6357–6369
17. Fahie, M., Romano, F. B., Chisholm, C., Heuck, A. P., Zbinden, M., and Chen, M. (2013) A non-classical assembly pathway of *Escherichia coli* pore-forming toxin cytolysin A. *J. Biol. Chem.* **288,** 31042–31051
18. Degiacomi, M. T., Iacovache, I., Pernot, L., Chami, M., Kudryashev, M., Stahlberg, H., van der Goot, F. G., and Dal Peraro, M. (2013) Molecular assembly of the aerolysin pore reveals a swirling membrane-insertion mechanism. *Nat. Chem. Biol.* **9,** 623–629
19. Petosa, C., Collier, R. J., Klimpel, K. R., Leppla, S. H., and Liddington, R. C. (1997) Crystal structure of the anthrax toxin protective antigen. *Nature* **385,** 833–838
20. Wai, S. N., Lindmark, B., Söderblom, T., Takade, A., Westermark, M., Oscarsson, J., Jass, J., Richter-Dahlfors, A., Mizunoe, Y., and Uhlin, B. E. (2003) Vesicle-mediated export and assembly of pore-forming oligomers of the enterobacterial ClyA cytotoxin. *Cell* **115,** 25–35
21. Benke, S., Roderer, D., Wunderlich, B., Nettels, D., Glockshuber, R., and Schuler, B. (2015) The assembly dynamics of the cytolytic pore toxin ClyA. *Nat. Commun.* **6,** 6198
22. Finder, V. H., Vodopivec, I., Nitsch, R. M., and Glockshuber, R. (2010) The recombinant amyloid-β peptide Aβ1–42 aggregates faster and is more neurotoxic than synthetic Aβ1–42. *J. Mol. Biol.* **396,** 9–18
23. Ellman, G. L. (1958) A colorimetric method for determining low concentrations of mercaptans. *Arch. Biochem. Biophys.* **74,** 443–450
24. Crespo, M. D., Puorger, C., Schärer, M. A., Eidam, O., Grütter, M. G., Capitani, G., and Glockshuber, R. (2012) Quality control of disulfide bond formation in pilus subunits by the chaperone FimC. *Nat. Chem. Biol.* **8,** 707–713
25. Rennie, R. P., Freer, J. H., and Arbuthnott, J. P. (1974) The kinetics of erythrocyte lysis by *Escherichia coli* haemolysin. *J. Med. Microbiol.* **7,** 189–195
26. Müller, B. K., Zaychikov, E., Bräuchle, C., and Lamb, D. C. (2005) Pulsed interleaved excitation. *Biophys. J.* **89,** 3508–3522
27. Wunderlich, B., Nettels, D., Benke, S., Clark, J., Weidner, S., Hofmann, H., Pfeil, S. H., and Schuler, B. (2013) Microfluidic mixer designed for performing single-molecule kinetics with confocal detection on timescales from milliseconds to minutes. *Nat. Protoc.* **8,** 1459–1474
28. del Castillo, F. J., Moreno, F., and del Castillo, I. (2001) Secretion of the *Escherichia coli* K-12 SheA hemolysin is independent of its cytolytic activity. *FEMS Microbiol. Lett.* **204,** 281–285
29. Ludwig, A., Bauer, S., Benz, R., Bergmann, B., and Goebel, W. (1999) Analysis of the SlyA-controlled expression, subcellular localization, and pore-forming activity of a 34-kDa haemolysin (ClyA) from *Escherichia coli* K-12. *Mol. Microbiol.* **31,** 557–567
30. Rojko, N., Kristan, K. Č., Viero, G., Žerovnik, E., Maček, P., Dalla Serra, M., and Anderluh, G. (2013) Membrane damage by an α-helical pore-forming protein, equinatoxin II, proceeds through a succession of ordered steps. *J. Biol. Chem.* **288,** 23704–23715
31. Kim, J. Y., Doody, A. M., Chen, D. J., Cremona, G. H., Shuler, M. L., Putnam, D., and DeLisa, M. P. (2008) Engineered bacterial outer membrane vesicles with enhanced functionality. *J. Mol. Biol.* **380,** 51–66
32. DeLano, W. L. (2010) *The PyMOL Molecular Graphics System*, version 1.3r1, Schrödinger, LLC, New York

SUPPLEMENTARY TABLE

Supplementary Table 1. Crystallographic data collection and model refinement statistics for CC6/264.

ClyA variant CC6/264	**Thr 2 – Val 302**	**Cys 6 – Val 302**
Crystal form		
Space group	$C222_1$ (20)	C2 (5)
Unit cell dimensions a,b,c (Å)	94.92, 125.53, 186.79; $\alpha = \beta = \gamma = 90°$	176.88, 48.44, 152.43; $\alpha = \gamma = 90°$, $\beta = 102.34°$
Data collection		
Wavelength (Å)	1.0	1.0
Resolution range (Å)	50.00 – 2.12	40.00 – 1.94
Unique reflections	63155 (9986)	85704 (12628)
Completeness (%)	99.5 (97.1)	91.0 (89.2)
R_{merge} (%)	6.4 (86.1)	8.0 (51.8)
I/σ	21.63 (3.10)	11.50 (2.55)
Wilson B factor ($Å^2$)	39.62	23.60
Model Statistics		
Refinement		
Resolution range (Å)	48.10 – 2.12	39.55 – 1.94
Reflections working/free sets	59151 / 3020	85693 / 2000
R_{work} /R_{free} (%)	18.51 / 23.08	17.60 / 21.79
RMS deviations		
Bonds (Å)	0.007	0.007
Angles (°)	0.888	0.903
Ramachandran plot		
Favoured (%)	99.19	99.48
Allowed (%)	0.81	0.52

SUPPLEMENTARY FIGURES

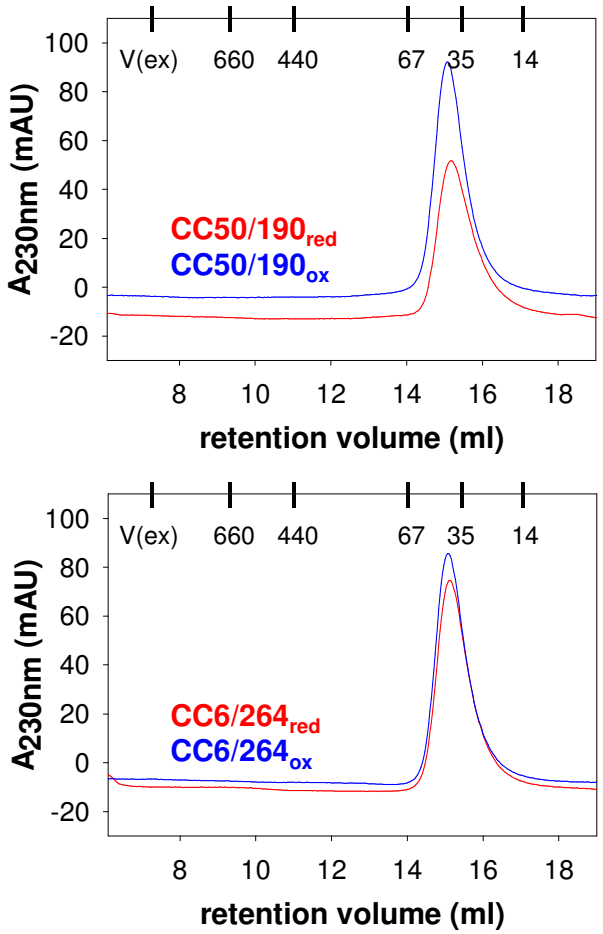

Figure S1. Gel filtration profiles of the reduced and oxidized ClyA variants CC50/190 and CC6/264 on a Superdex 200 10/300 column at pH 7.3, showing the monomeric state of the variants in both redox forms. Due to its elongated shape, the ClyA monomer (34.6 kDa for the $(His)_6$-tagged protein) shows a slightly increased apparent molecular mass of ~40 kDa in gel filtration experiments. The retention volumes of molecular mass standards (in kDa) and the exclusion volume (V_{ex}) are indicated.

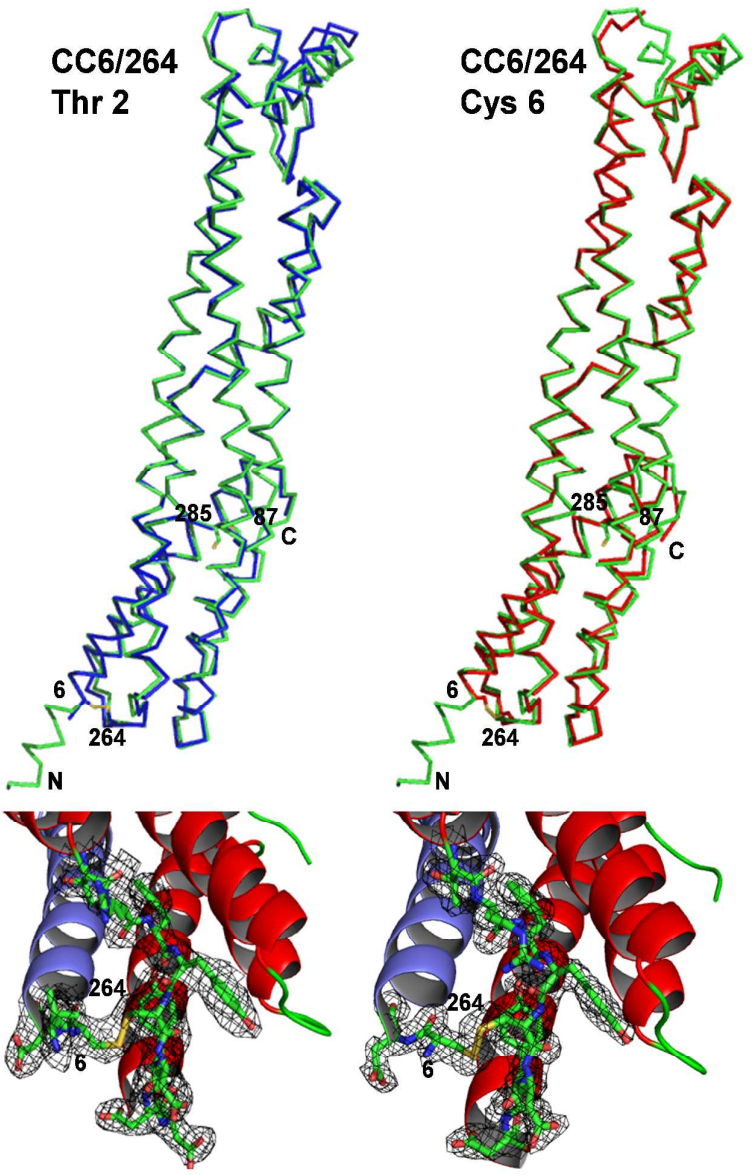

Figure S2: Ribbon representations of structural alignments of ClyA wt (pdb ID 1QOY) with chains from crystal structures of ClyA CC6/264 containing the artificial disulfide bond 6-S-S-264 (top). Structural alignments were performed using DaliLite. The positions of the wild type cysteines 87 and 285 and the engineered cysteines 6 and 264 are indicated. Left: 2.12 Å crystal structure of ClyA CC6/264 (2–303; blue) aligned with the 2.0 Å crystal structure of ClyA wt (green). Right: 1.94 Å crystal structure of ClyA CC6/264 (6–303; red) aligned with the 2.0 Å crystal structure of ClyA wt (green). Sections of both structures depicting the artificial disulfide bond (bottom). The electron density maps (contoured at 1.0 sigma) are shown for residues Val5–Asp7 (2–303, left) or Cys6 - Asp7 (6–303, right) and Thr260–Asp268. Figures were produced with PyMOL.

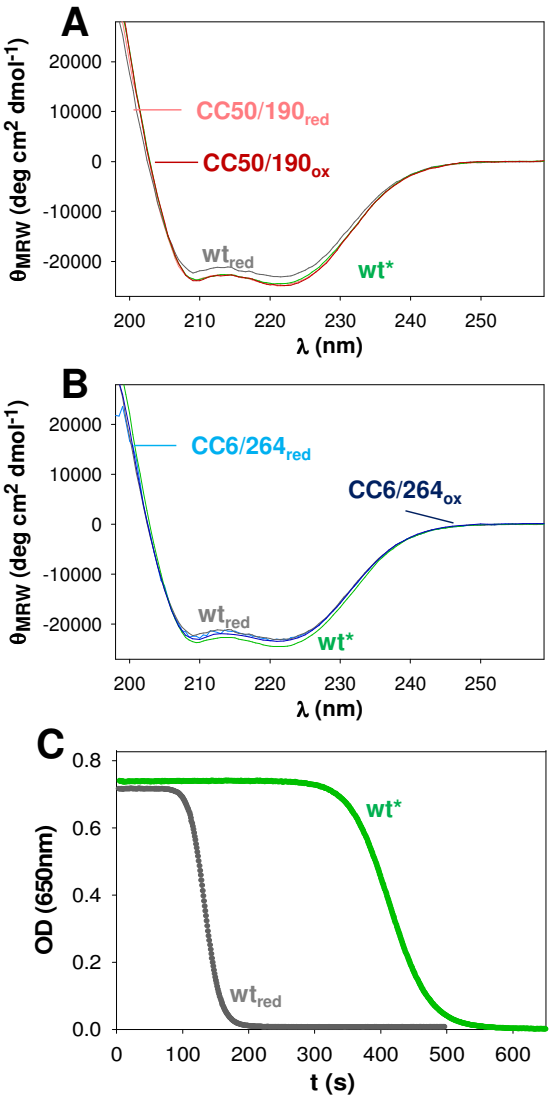

Figure S3: Far-UV CD spectra of ClyA and ClyA variants with the engineered disulfide bonds 50–190 and 6–264 are highly similar. Spectra of reduced wt ClyA, the cysteine-free pseudo wild type (wt*), and the variants CC50/190 and CC6/264 (8.9 µM) at pH 7.3 and 22 °C are shown. A: Far-UV CD spectra of the reduced wt, wt* and the oxidized and reduced forms of the variant CC50/190. B: Far-UV CD spectra of wt, wt* and the oxidized and reduced forms of the variant CC6/264. C: Comparison of the hemolytic activity at 37 °C and pH 7.3 of reduced wt ClyA and wt*. Reactions were initiated by mixing horse erythrocytes at a density of 2 x 10^6 cells/ml with the respective ClyA protein (10 nM), and cell lysis was followed via the decrease in optical density at 650 nm.

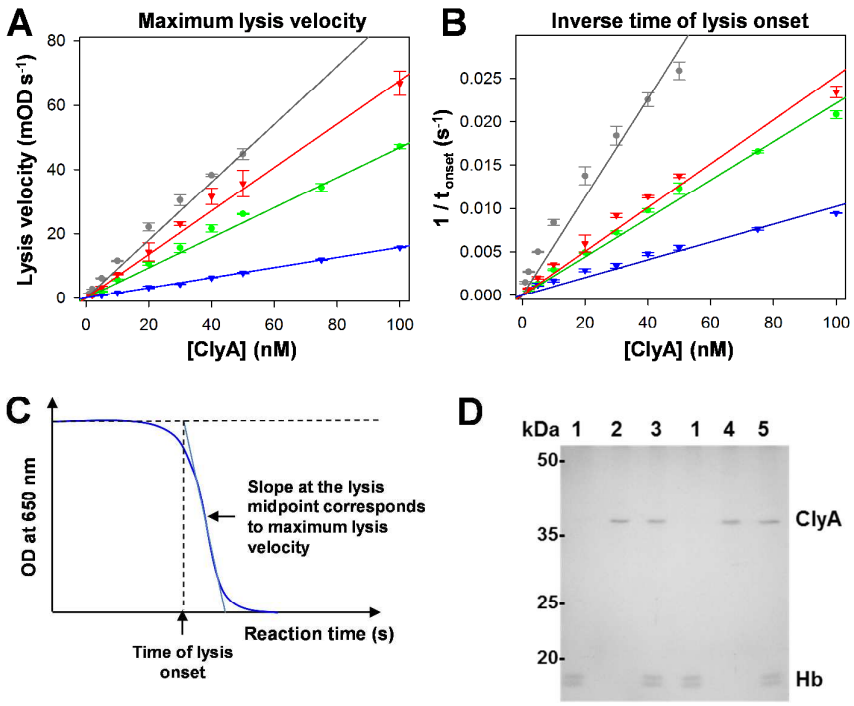

Figure S4: Evaluation of different parameters for quantifying the specific hemolytic activity of ClyA variants (see also Table S2). All measurements were performed at 37 °C , pH 7.3 with an initial density of 2 x 10^6 horse erythrocytes/ml, and initiated by adding varying concentrations (1–100 nM) of the respective ClyA monomer (gray: wt_{red}; green: wt*; red: $CC50/190_{red}$; blue: $CC6/264_{red}$). Error bars show the standard deviation from three independent measurements. The following parameters (see panel C for definitions) were plotted against the ClyA monomer concentrations: A: maximum lysis velocity; B: inverse time of lysis onset; C: Scheme defining the parameters for correlating hemolytic activity with ClyA concentration. D: The oxidized variants $CC50/190_{ox}$ and $CC6/264_{ox}$ (100 nM each) stay in the supernatant after incubation with erythrocytes (10^7 cells per ml) at 37 °C for 10 min and erythrocyte sedimentation by centrifugation. A Coomassie-stained SDS-polyacrylamide gel with samples (20 µl each) of the following solutions is shown: (1) erythrocyte supernatant; (2) 100 nM $CC50/190_{ox}$; (3) $CC50/190_{ox}$ in the supernatant after incubation with erythrocytes and centrifugation. (4) 100 nM $CC6/264_{ox}$; (5) $CC6/264_{ox}$ in the supernatant after incubation with erythrocytes and centrifugation. Hb, released hemoglobin chains from a small fraction of lysed erythrocytes.

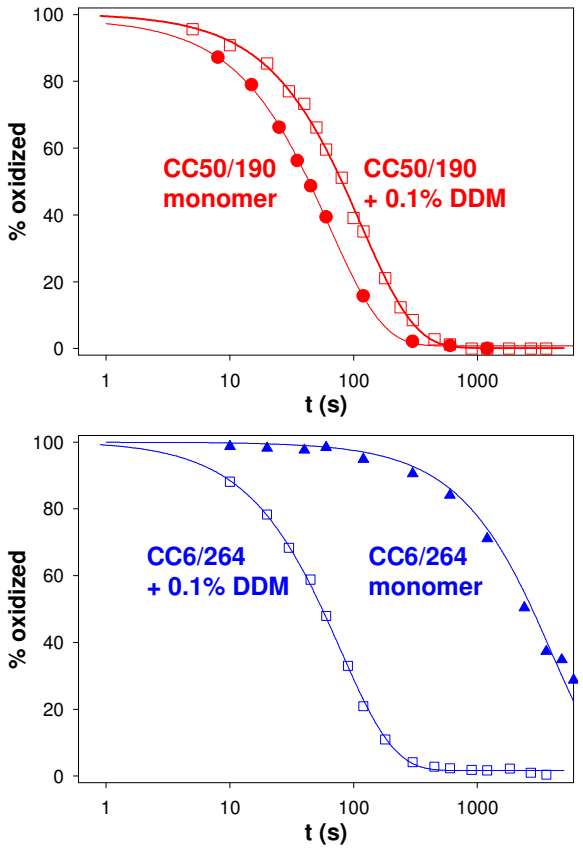

Figure S5: Comparison of the sensitivity for reduction by DTT of the oxidized ClyA variants CC50/190 (red, upper panel) and CC6/264 (blue, lower panel) in their monomeric state in the absence of DDM, and the DDM-induced intermediate state (I^{SS}). Reduction reactions were performed at 37 °C and pH 7.3 with 10 mM DTT. The reactions were acid-quenched after different times, and the oxidized and reduced proteins were separated by reversed-phase HPLC. The fraction of oxidized protein (determined with peak integration) was plotted against the reaction time and data were fitted to pseudo-first-order kinetics (solid lines). Closed circles: Reduction of oxidized monomers; open squares: Reduction of the I^{SS} state after incubation for 30 min in 0.1% DDM. The deduced second order rate constants are: CC50/190 monomer: 1.6±0.1 M^{-1} s^{-1}; CC50/190 + 0.1% DDM (I^{SS}-state): 0.86±0.1 M^{-1} s^{-1}; CC6/264 monomer: 2.4± 0.1x10^{-2} M^{-1} s^{-1}; CC6/264 + 0.1% DDM (I^{SS}-state): 1.2 ± 0.1 M^{-1} s^{-1}. The results show that the engineered disulfide in the variant CC6/264 is deprotected 50-fold from reduction in the trapped intermediate I^{SS}, while the disulfide in the variant CC50/190 is protected 2-fold upon formation of I^{SS}.

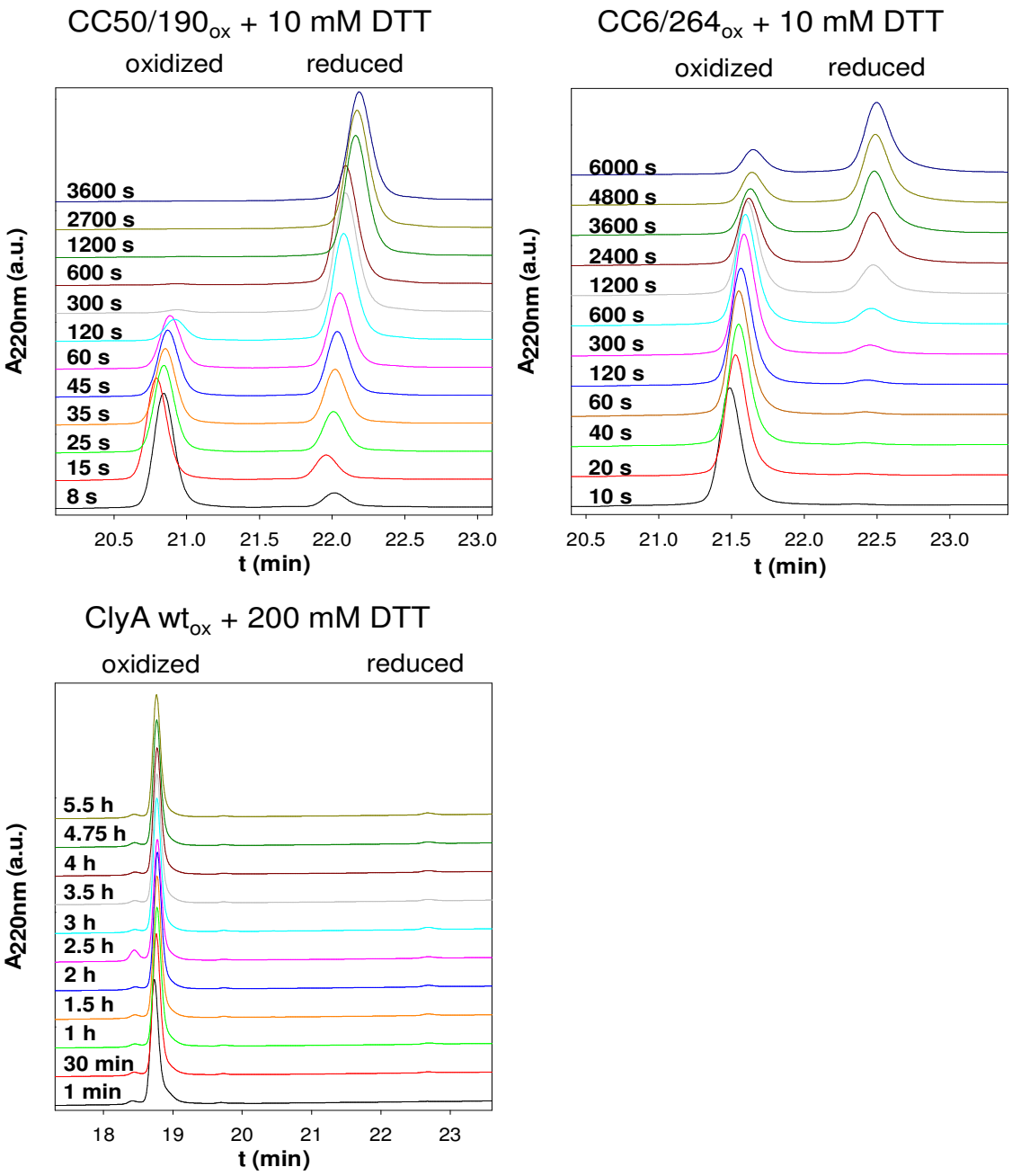

Figure S6: Reduction of oxidized ClyA wt and the oxidized variants CC50/190 and CC6/264 (5 µM each) with 200 mM DTT (wt) or 10 mM DTT (variants) at 37 °C and pH 7.3, and reversed-phase HPLC separation of oxidized and reduced protein after acid-quenching at different reaction times. Proteins were separated on a Zorbax 300SB C8 column (Agilent), eluted with a linear acetonitrile gradient (30–80% (v/v) in 0.1% trifluoroacetic acid) and detected via their absorbance at 220 nm.

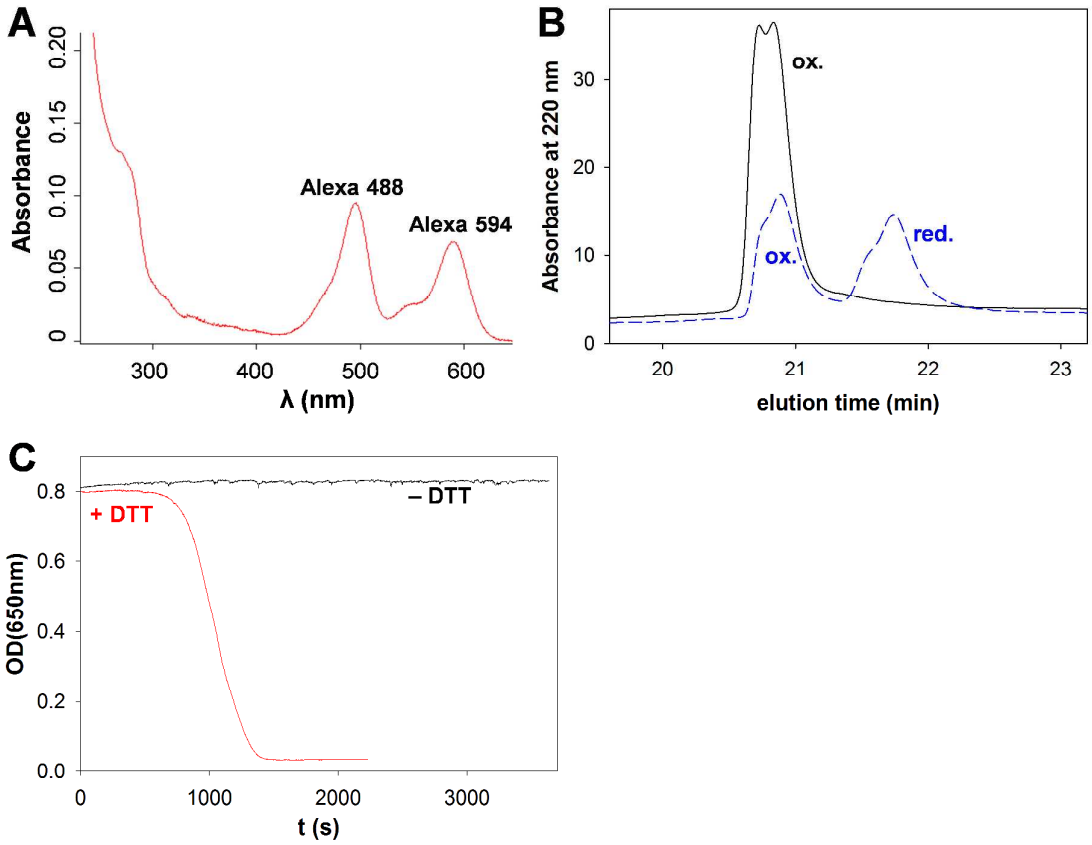

Figure S7: Verification of donor/acceptor labeling of the ClyA variant CC6/264 Q56C E252C and formation of the C6-C264 disulfide bond. A: Absorbance spectrum of the oxidized, double labeled protein after the final gel filtration step. Concentrations of protein-bound Alexa 488 and 594 were 1.30 µM and 0.74 µM, respectively (see Materials and Methods for details). The protein concentration (average of Alexa 488 and Alexa 594 concentration) was 1.02 µM. B: Reversed-phase HPLC profile of double labeled, oxidized ClyA CC6/264 Q56C E252C used in all single-molecule experiments (solid, black line). The dotted, blue line corresponds to a preparation where the second labeling step was performed with an excess of Alexa 594 over protein so that the cysteine pair C6/C264 also became partially labeled and only about 50% of the molecules could form the C6/C264 disulfide bond. The chromatogram shows that oxidized and reduced protein can be separated well under the HPLC conditions, and that the preparation of double labeled ClyA CC6/264 Q56C E252C (black line) used for single molecule experiments was oxidized quantitatively. C: Reduction of the disulfide bond C6/C264 by DTT regenerates hemolytic activity

of the donor/acceptor labeled variant CC6/264 Q56C E252C (+DTT, red line), while the disulfide-intact variant (–DTT, black line) lacks hemolytic activity. Horse erythrocytes (2 x 10^6 cells/ml) were mixed with 20 nM ClyA at 37 °C and pH 7.3, and the decrease in optical density at 650 nm as a consequence of erythrocyte lysis was recorded. The red hemolysis curve represents the reaction started by addition of 20 mM DTT to the erythrocyte suspension pre-incubated with oxidized, donor/acceptor labeled ClyA CC6/264 Q56C E252C.

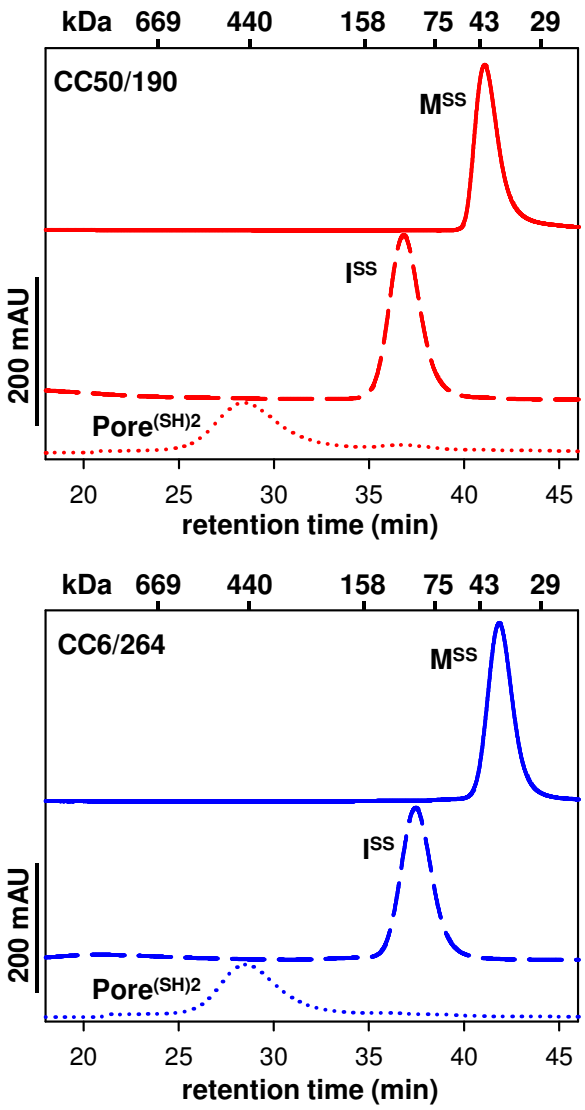

Figure S8: Size exclusion chromatography on Superdex 200 of the I^{SS} states (dashed lines) of ClyA $CC50/190_{ox}$ (top panel, red lines) and $CC6/264_{ox}$ (bottom, blue lines) at 22°C and pH 7.3. The I^{SS} states were populated by incubation of the oxidized variants in 0.1% DDM for 1.5 hours prior to chromatography in PBS buffer containing 0.1% DDM. As a control, gel filtration runs were also performed with the respective monomers (M^{SS} states, solid lines) in PBS without DDM, and with the assembled pore complexes of the reduced variants ($Pore^{(SH)2}$, dotted lines) in PBS, 0.1% DDM. The retention times of molecular mass standard proteins are indicated at the top of each panel. The I^{SS} states of both variants eluted at retention times expected for a ClyA monomer embedded in a DDM micelle (34 kDa + 70 kDa).

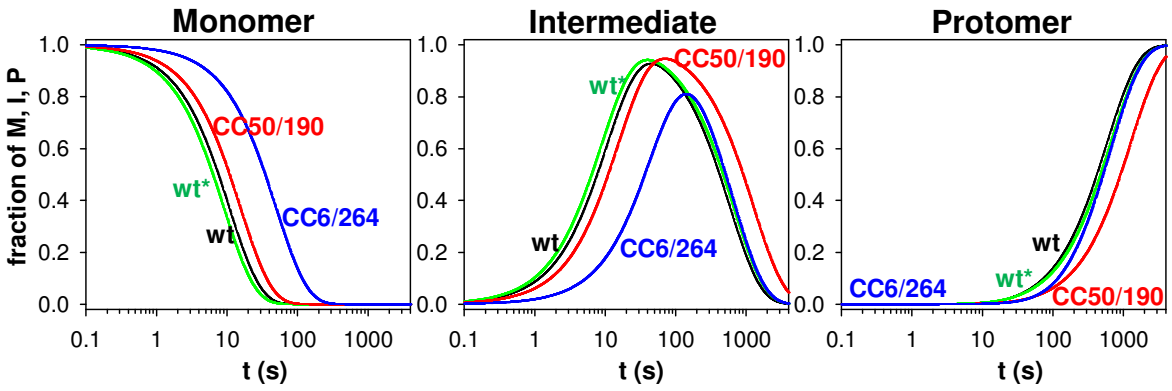

Figure S9: Simulation of the fractions of monomer, intermediate, and protomer of ClyA wt, wt* and the reduced variants CC50/190 and CC6/264 derived from the rate constants k_{MI} and k_{IP} that were obtained by ANS fluorescence measurements (cf. Figure 6 and Table 1). The intermediates of wt, wt*, and CC50/190 are maximally populated to more than 92%. The intermediate of CC6/264 is maximally populated to 81%.